ELSEVIER

Physics of the Earth and Planetary Interiors 127 (2001) 109–143

PHYSICS OF THE EARTH AND PLANETARY INTERIORS

www.elsevier.com/locate/pepi

"Detached" deep earthquakes: are they really?

Emile A. Okal

Department of Geological Sciences, Northwestern University, Evanston, IL 60208, USA

Received 28 March 2000; accepted 27 July 2000

Abstract

We use primarily the generation of acoustic T waves into the ocean by deep seismic sources to investigate the propagation of high-frequency seismic energy from the bottom of subduction zones to the shoreline at the earth's surface. Conversion from shear waves to oceanic acoustic waves can be used as a proxy for the existence of a continuous slab featuring low anelastic attenuation. With the help of other techniques, such as the estimation of Q from S-to-P spectral amplitude ratios, we examine systematically a number of regions where earthquakes have been described as "detached". We establish the mechanical continuity of the slab to the hypocenters of the 1990 Sakhalin and 1982 Bonin events, which occurred several hundred kilometers in front of the mainstream seismic zone. The study of the 1989 Paraguay shock is inconclusive, probably due to its much smaller size. The vertical continuity of the South American slab through its aseismic depth range is verified, and a similar situation probably exists in Java. Attenuation data suggests that the deep Spanish earthquakes occur within a vertically large segment of colder material, and a similar situation may exist in Colombia. The only clearly detached deep events with no mechanical connection to the surface make up the Vityaz cluster, under the North Fiji Basin. Based on a variety of geophysical evidence, the small deep earthquakes under New Zealand are likely to take place in a detached blob at least 350 km below the termination of mainstream seismicity. These results support a model integrating buoyancy forces over a long continuous slab as the source of the down-dip compressional stresses observed in large earthquakes at the bottom of the transition zone.

Keywords: Detached; Deep earthquakes; High-frequency seismic energy

1. Introduction and background

This paper studies a number of selected deep earthquakes, often described as "detached" because of the discontinuous character of seismicity at the bottom of the relevant subduction zones. Our principal tool of investigation are the T phases received at teleseismic distances across the ocean following these events; we are motivated by the fact that T waves can be channeled by the SOFAR low-velocity waveguide (Ewing et al., 1946) only at frequencies $f > 2.5$ Hz, and that their excitation, thus, expresses the ability for the earthquake to efficiently send high-frequency seismic energy, convertible into T waves, to the coastal area. We conclude that several such earthquakes can be better described as occurring in warped but continuous sections of the Wadati–Benioff zone (WBZ). We also show on several examples that T waves are indeed routinely recorded from large deep earthquakes at the bottom of subduction zones.

In a previous study concerned with the 1994 Bolivian earthquake (Okal and Talandier, 1997, 1998) (hereafter Paper I), we showed that the T phases it generated had to be converted from high-frequency S waves, which in turn required a path with low shear attenuation from the hypocenter to the water

E-mail address: emile@earth.nwu.edu (E.A. Okal).

0031-9201/01/$ – see front matter
PII: S0031-9201(01)00224-2

column, which could be explained only if a thermally and hence mechanically continuous slab extends upwards from the 1994 hypocenter. This observation was of particular interest since the Bolivian earthquake occurred in a region with no previous record of seismicity deeper than 280 km, between the Peruvian and south Bolivian–Argentinian deep clusters (Kirby et al., 1995). The combination of the 1994 seismicity (including aftershocks of the 9 June event), of several recent earthquakes, and of the efficient propagation of high-frequency regional S waves (with Q_μ estimated as at least 800 in Paper I), indicates that rather than being torn, the slab is merely warped along a jog linking the Peruvian and Argentinian segments, and remains continuous both laterally and vertically.

A conclusion of Paper I, substantiated by the examination of spectra of regional S waves, was that the existence of an $S \rightarrow T$ conversion from a deep earthquake at the bottom of a subduction zone can be viewed as a proxy for a mechanically continuous slab, an especially valuable result in the presence of a gap of activity in the WBZ. Similarly, a recent study by Mele (1998) in the Calabrian arc, has estimated $Q_\mu \approx 1000$ and calculated that a 25-km gap in the continuity of the slab would suffice to eradicate high-frequency (6 Hz) S waves, such resolution being of course much finer than that of even the best tomographic models. Armed with this technique, we focus in this paper on a number of regions where several earthquakes have been previously described as "detached" in the literature. Their geographical layout can take several forms which we now examine in detail.

1.1. Wadati–Benioff zones with depth gaps

Ever since the pioneering work of Benioff (1949), it was noticed that seismicity in several slabs is not downward continuous, prompting early authors to propose that the slab may be mechanically "broken", with earthquakes taking place in individual blobs of sinking lithosphere, (e.g., Isacks and Molnar, 1971; Wortel, 1984). The primary example of such a geometry is South America, where seismicity gaps exist between depths of 337 and 502 km in northern Argentina, and between 211 and 506 km in Peru–Brazil (Engdahl et al., 1998), while farther North, activity below 292 km is documented only in the form of three very large, very deep events in 1921, 1922 and 1970 (Okal and Bina, 1994), and of three similarly very deep but very small 1997 shocks scattered between the 1921–1922 hypocentral area and the northern end of the Peru–Brazil deep cluster (Okal and Bina, 2001). The occurrence of the great 1994 Bolivian earthquake, its aftershocks, and several recent earthquakes (14 March 1995; 28 November 1997) indicated that while the slab itself must be continuous horizontally between the foci of abundant deep seismicity in Peru–Bolivia and Argentina, it does feature a vertical gap in seismicity in central Bolivia from 280 to 566 km depth. Another example of a gap in seismicity with depth is the Java WBZ, West of 115°E, where no earthquakes are known between 338 and 470 km, (e.g., Kirby et al., 1996).

1.2. Outboard earthquakes

Lundgren and Giardini (1994) have reviewed a number of cases of earthquakes occurring several hundred km in front of the general trend of the WBZ in the relevant subduction zone. The most prominent examples are the 1990 Sakhalin, 1982 Bonin Islands and 1989 Paraguay events. Under the South Fiji Basin, West of Tonga, a number of narrow fingers of seismicity extending as much as 700 km in front of the WBZ have also been documented (Okal and Kirby, 1998; Brudzinski and Chen, 1998).

1.3. The Vityaz deep cluster

Under the North Fiji Basin, Okal and Kirby (1998) have analyzed in detail a large cluster of frequent, relatively small earthquakes at depths of 570–660 km. They concluded that these events take place in a piece of slab severed from a deactivated subduction system and lying recumbent on the bottom of the transition zone.

1.4. The small deep earthquakes under New Zealand

The bottom limit of the WBZ rises regularly from 650 km under the Kermadec Islands at 30°S to 260 km under Cook Strait at 41°S. It is probable that this process is controlled by the reduction in thermal parameter Φ (Kostoglodov, 1989; Kirby et al.,

1991) resulting from a slower convergence rate as one moves southwards closer to the pole of rotation of the Pacific–Australian plate system (DeMets et al., 1990). However, a few earthquakes have been documented at depths of 570–622 km under the North Island of New Zealand at 39°S (Adams, 1963; Adams and Ferris, 1976), where mainstream seismic activity stops at 250 km. Additional events in 1991–1998 confirm the existence of this intriguing seismic cluster. Incidentally, it should be emphasized that this situation is not unique among subduction zones, and that individual events are occasionally reported at depths greater than that of cessation of abundant seismicity at the tip of WBZs. A striking example is the South Sandwich system, where seismicity is confined to the upper 200 km of slab, but where rare events can occur down to ∼300 km (the latest one on 5 October 1997; $h = 273$ km; $m_b = 6.3$). However, we do not address such cases of detached earthquakes at intermediate depths in the present paper.

1.5. The deep Spanish earthquakes

The origin of the large 1954 shock at 627 km, studied in detail by Chung and Kanamori (1976), remains to this day a largely unresolved puzzle; only three events are known in its vicinity, in 1973, 1990, and 1993. Intermediate seismicity is known to the SSW, down to ∼135 km depth (Mezcua and Rueda, 1997).

In all above geometries, the question arises whether the deep seismicity occurs in blobs of sinking lithosphere actually detached from the main slab, or rather is merely a result of a change in geometrical or thermomechanical properties controlling the existence or the release of ambient stresses in an otherwise physically continuous slab. The answer to this question is of course of great importance for our understanding of the dynamics of the subduction process.

2. Previous approaches

Three main lines of evidence have previously been used to explore the nature of gaps in deep seismicity: first, experiments in seismic tomography have been used to infer thermal continuity for the South American slab (Engdahl et al., 1995), to suggest at least partial deflection of the latter's southern segment, as well as of the Izu–Bonin slab (van der Hilst et al., 1993), and to image a flat lying extension of the Tonga slab under the South Fiji Basin (van der Hilst, 1995), where it hosts the seismic fingers described by Okal and Kirby (1998). Also, in the case of the 1982 "detached" event in the Bonin Islands, Okino et al. (1989) used travel-time residuals at Japanese stations to argue for the presence of fast material in the event's immediate vicinity.

Second, Isacks and Molnar (1971) and Huang et al. (1998) (among others) have noted the coherence of focal geometries of events below the depth gap in South America, notably in Argentina, where the mechanisms express down-dip compression, arguing for the mechanical continuity of the slab through its aseismic segment. The latter was explained by Engebretson and Kirby (1992) as involving an age discontinuity in the downgoing lithosphere. Conversely, Okal and Kirby (1998), noting the wide variety of focal mechanisms in the Vityaz deep cluster, have argued for its being mechanically unrelated to any shallower structures. Lundgren and Giardini (1994) also presented evidence that outboard events have mechanisms differing from those of neighboring events in the mainstream WBZ.

Finally, a number of regional studies have identified high-frequency *S* waves in various subduction zones, some of them with seismicity gaps. In particular, in South America, Sacks (1969), and later Isacks and Barazangi (1973), Snoke et al. (1974a) and James and Snoke (1990) used this technique to propose the mechanical continuity of the slab through the aseismic depth gap, although Snoke et al. (1974b) also proposed an underside reflection on the subducting slab as an alternate explanation for the late phases. Mooney (1970) in New Zealand, Barazangi et al. (1972) in Tonga, and Mele (1998) in the Calabrian arc, also used similar techniques. van der Hilst and Snieder (1996) modeled the propagation of high-frequency *P* waves through a three-dimensional model of lateral heterogeneity under New Zealand and concluded that their observation almost certainly requires the continuity of the slab. Our approach will be conceptually similar, building on the same principle, i.e. that high-frequency *S* waves need a cold, continuous medium to propagate from the bottom of the WBZ, but will use a different observational strategy, and be global in scope.

3. Dataset and methodology

In this general framework, we investigate in the present study the propagation of high-frequency *S* waves up slab from a number of deep earthquakes located in targeted subduction zones. We focus on the process of generation of *T* waves in the oceanic column, complemented occasionally by the direct spectral analysis of regional *S* waves. We refer to Paper I for a description of the general techniques used.

3.1. Dataset

In the present study, we rely on the following datasets:

- for recent (post-1989) events, IRIS continuous broad-band channels;
- for a few events in 1994–1996, continuous broad-band records of the Micronesian Seismic Experiment (Richardson, 1998);
- since ∼1996, continuous hydrophone channels of the Wake Hydrophone array, available from the Prototype International Data Center;
- from ∼1975 to 1989, GDSN short-period channels (usually available through the IRIS Data Center), in general, the recording of these channels was triggered, and only *P* (and occasionally *S*) windows are available, which can constitute a very significant handicap for the study of *T* waves;
- analog (paper) continuous records at the French Polynesia seismic array, available since 1962, with

Table 1
Seismic events used in the *T* wave study

Code	Name	Island			Coordinates		Distance to closest conversion point[a]
		Name	Chain	Nature[b]	°N	°E	
French Polynesia							
PMO	Pomariorio	Rangiroa	Tuamotu	a	−15.017	−147.906	50 m
TPT	Tiputa	Rangiroa	Tuamotu	a	−14.984	−147.619	50 m
REAO	Reao	Reao	Tuamotu	a	−18.51	−136.40	50 m
MEH	Mehetia	Mehetia	Society	h	−17.875	−148.066	200 m
PPT	Pamatai	Tahiti	Society	h	−17.569	−149.574	8 km
TET	Tetiaroa	Tetiaroa	Society	a	−16.996	−149.586	50 m
RKT	Rikitea	Mangareva	Gambier	e	−23.118	−134.972	12 km
TBI	Tubuai	Tubuai	Austral	h	−23.349	−149.461	8 km
Hawaii							
KAA	Kalahiki	Hawaii	Hawaii	h	19.266	−155.871	7 km
HUL	Heiheiahulu	Hawaii	Hawaii	h	19.419	−154.979	7 km
KIP	Kipapa	Oahu	Hawaii	h	21.420	−158.020	22 km
Other							
RPN	Rapa Nui	Easter		h	−27.127	−109.334	8 km
KOS	Kosrae	Kosrae	Caroline	h	5.324	163.009	6 km
TKK	Moen	Chuuk	Caroline	e	7.447	151.887	19 km
NAU	Nauru	Nauru		u	−0.509	166.932	200 m
RAR	Rarotonga	Rarotonga	Cook	h	−21.210	−159.770	10 km
AFI	Afiamalu	Opulu	Samoa	h	−13.910	−171.780	18 km
GUMO	Guam	Guam	Mariana	b	13.588	144.866	12 km
COCO	Cocos Island	Cocos	Keeling	a	−12.190	96.835	2 km
WK30	Wake Hydrophone				19.410	167.499	
SYP	Santa Ynez Peak, California				34.527	−119.978	82 km
SNCC	San Nicolas Island, California				33.248	−119.524	73 km
SCZ	Santa Cruz, California				36.60	−121.40	58 km
PET	Petropavlovsk–Kamchatskiy, Russia				53.017	158.650	36 km
HOPE	Hope, South Georgia				−54.824	−36.488	58 km

[a] This is the minimum distance to a conversion point, but depending on the geometry of arrival, the actual distance used to estimate a correction may be larger.

[b] a: atoll; h: high island (volcanic); e: eroded high island inside large lagoon; u: uplifted atoll; b: uplifted fore-arc basement.

high-frequency (T wave) channels (Talandier and Kuster, 1976) available since the mid-1970s;
- analog (paper and develocorder film) continuous records of the Hawaii Volcano Observatory (HVO) short-period array;
- analog (paper) continuous records of the Caltech short-period network in southern California;
- analog (micro-film) continuous short-period records of the WWSSN, they suffer from the often mediocre gains used at ocean island stations.

It should be emphasized that signal processing methods, such as high-pass filtering and spectrogram analysis can be applied routinely only to digital datasets. In the case of analog records, we were occasionally able to hand-digitize time series for further processing, after enlarging the record several times using a magnifying photocopier. The quality of the resulting time series remains low, and they can be used only at the lower end of the frequency window of interest here ($f \leq 3$ Hz).

Whenever possible, we use in this study T wave receiving stations located on atolls characterized by steep reefs optimizing the acoustic-to-seismic conversion on the receiver side (Talandier and Okal, 1996). Table 1 lists parameters for stations used in the present work, and Table 2 lists events studied with the T wave technique.

3.2. Station corrections

As detailed in Paper I, and based upon the work of Talandier and Okal (1998), we introduce station corrections to compensate for the faster propagation inside the insular or continental structure after conversion back into seismic energy on the receiver side. These corrections are unnecessary in the case of atoll sites such as the Rangiroa stations in French Polynesia, or for very small high islands whose dimensions can be neglected (Mehetia, Pitcairn).

3.3. Example and methodology

As intriguing as this situation may be, given that their sources are de facto removed from the oceanic water mass, the excitation of T phases by deep earthquakes is the rule rather than the exception. Fig. 1 shows a typical example of T wave recorded at station RPN, (Easter Island) following the earthquake of 21 July 1994 under the Primorye province of eastern Russia. This event is discussed in more detail in Appendix A, but we use this record here to describe the methodology of the present study.

The two T wave arrivals are easily extracted by filtering in Fig. 1b, and further resolved by the spectrogram in frame (c). The T phase is clearly composed of two arrivals, with maxima separated by 90 s, at 21:09:14 and 21:10:44 GMT, respectively. We use a station correction of 4 s to account for 11 km of on-land propagation at Easter Island following acoustic-to-seismic conversion (Talandier and Okal, 1998) for final times of 21:09:18 and 21:10:48, with a precision estimated at ± 5 s. In Fig. 2, which is conceptually similar to Figs. 3–5 of Paper I,[1] we study the residual (defined as the difference between the observed arrival time of the T phase and the arrival time computed from a modeled conversion), as a function of the latitude of the point of conversion along the Japan–Kuril shoreline. The fundamental result from Fig. 2 is that no $P \rightarrow T$ conversion anywhere along the shore can explain the second arrival, which remains always more than 1 min late. On the other hand, it is easily explained by an $S \rightarrow T$ conversion taking place at 41.5°N, 141.9°E, which corresponds to a concave bight in the 1200 m isobath at the Hokkaido corner (Fig. 3). Note that the first arrival can be explained by a $P \rightarrow T$ conversion at essentially the same location (it could also, conceivably, be explained by an $S \rightarrow T$ conversion off Cape Erimo). We conclude that the two pulses in the T phase correspond to $P \rightarrow T$ and $S \rightarrow T$ conversions, respectively, generated by a scatterer at the Hokkaido corner.

The $S \rightarrow T$ conversion is observed in Fig. 1 to be of larger amplitude than the $P \rightarrow T$ one; this is found to be a common occurrence, which can be justified along the following arguments: first, as is well known from elementary seismic theory, (e.g., Okal, 1992), the generation of S waves by a double-couple is $(\alpha/\beta)^3$ times more efficient (5.2 times in a Poisson solid) than that of P waves. This results in teleseis-

[1] Due to a production error, Figs. 3 and 4 were permuted in (Okal and Talandier, 1997). The figures were reprinted correctly in (Okal and Talandier, 1998).

Table 2
Seismic events used in the T wave study

Date (D M (J) Y)	Origin time (GMT)	Hypocenter			Published CMT solution	
		Latitude (°N)	Longitude (°E)	Depth (km)	M_0 (10^{27} dyn cm)	ϕ, δ, λ (°)
Okhotsk–Sakhalin–Primorye						
30 AUG (242) 1970	17:46:09.0	52.38	151.60	645	1.1	229, 78, 284
5 SEP (248) 1970	07:52:27.9	52.10	150.99	561	0.07	4, 79, 281
29 JAN (029) 1971	21:58:05.4	51.73	150.95	524	0.25	31, 73, 255
10 JUL (192) 1976	11:37:12.8	47.36	145.72	421	0.02	64, 81, 263
21 DEC (355) 1975	10:54:17.7	51.84	151.75	545	0.21	44, 77, 265
21 JUN (172) 1978	11:10:38.2	47.98	149.01	403	0.07	185, 85, 116
1 FEB (032) 1984	07:28:27.8	49.10	146.31	581	0.04	231, 85, 83
18 MAY (138) 1987	03:07:34.7	49.12	147.39	552	0.17	50, 83, 270
12 MAY (132) 1990[a]	04:50:08.7	49.04	141.85	605	0.82	172, 29, 210
21 JUL (202) 1994	18:36:31.7	42.34	132.87	471	1.1	64, 34, 178
Izu–Bonin–Marianas						
31 JAN (031) 1973	20:55:53.1	28.18	138.86	506	0.25	327, 79, 308
13 MAY (133) 1977	11:13:31.2	28.12	139.73	440	0.06	342, 72, 286
18 MAY (138) 1979	20:18:01.1	23.94	142.66	581	0.06	57, 47, 267
4 JAN (004) 1982	06:05:01.3	17.92	145.46	595	0.07	167, 58, 271
4 JUL (185) 1982[a]	01:20:07.6	27.92	136.48	552	0.12	80, 80, 248
6 MAR (066) 1984	02:17:21.1	29.60	139.110	446	1.4	332, 88, 290
5 AUG (217) 1990	01:34:57.5	29.48	137.500	520	0.06	296, 87, 322
23 AUG (235) 1995	07:06:02.6	18.88	145.30	599	0.46	136, 42, 242
16 MAR (076) 1996	22:04:06.2	28.98	138.94	477	0.11	68, 23, 197
Argentina–Paraguay						
21 DEC (355) 1983	12:05:06.3	−28.19	−63.17	602	0.27	202, 14, 115
28 FEB (059) 1989[a]	13:01;57.6	−23.11	−61.47	569	0.07	194, 24, 290
23 JUN (174) 1991	21:22:28.9	−26.80	−63.35	558	0.86	162, 68, 256
29 APR (119) 1994	07:11:30.3	−28.51	−63.22	566	0.25	169, 71, 260
10 MAY (130) 1994	06:36:28.4	−28.50	−63.10	600	0.28	256, 10, 183
19 AUG (231) 1994	10:02:51.8	−26.72	−63.42	563	0.06	159, 73, 253
Bolivia						
9 JUN (160) 1994	00:33:16.2	−13.841	−67.553	631	26	302, 10, 300
Colombia						
31 JUL (212) 1970	17:08:05.2	−1.46	−72.56	651	21	148, 58, 261
Vityaz						
13 APR (103) 1995	02:34:38.0	−13.45	170.43	637	0.021	312, 45, 287
New Zealand						
14 SEP (257) 1991	14:14:42.0	−39.180	174.434	602		

[a] The three outboard events studied by Lundgren and Giardini (1994).

mic S classically having larger amplitudes than P at typical long periods (10 s and above). At the high frequencies used in this study ($\omega > 20$ rad/s), teleseismic S waves are generally eradicated by anelastic attenuation, but propagation over a short distance (≈1000 km) up a cold slab with high Q_μ (≈800) can result in S waves of greater amplitude than P at the conversion point.

In addition, the radiation pattern of S waves up the slab can be more favorable that than of P for the particular focal mechanism involved. Also, Talandier and Okal (1998) have shown in the idealized case of a planar shore dipping at a constant angle that $S \rightarrow T$ conversions can be favored over $P \rightarrow T$ for a wide range of combinations of shore dips and ray incidences.

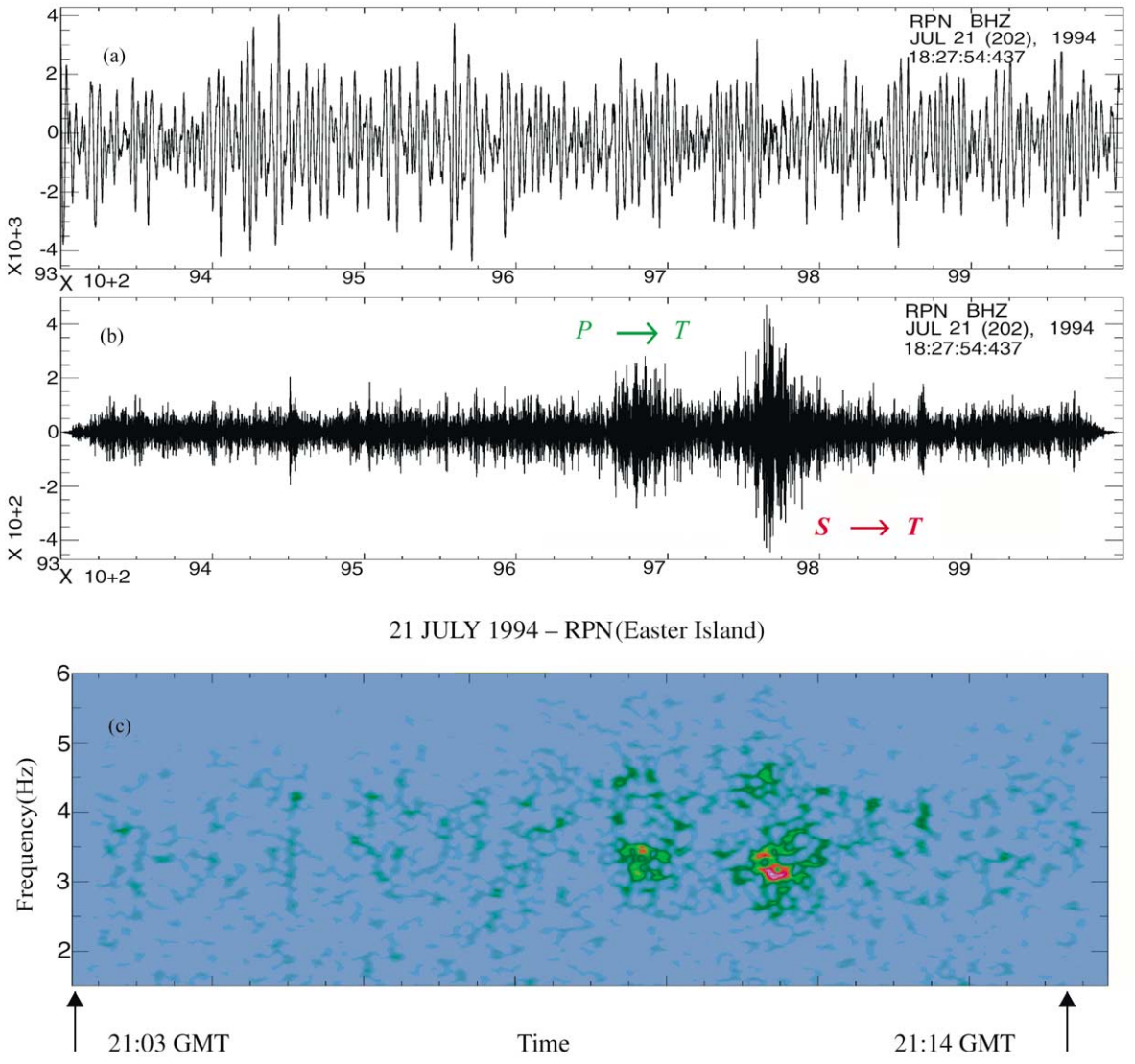

Fig. 1. Typical example of a teleseismic record of T wave from a deep earthquake (Primorye event of 21 July 1994 recorded at Easter Island (RPN)). The epicentral distance is 127.8°, and the oceanic path of the acoustic wave 13,450 km. (a) Original broad-band record. (b) High-pass filtered record ($f \geq 1.5$ Hz). Note the two strong arrivals interpreted as $P \rightarrow T$ and $S \rightarrow T$ conversions at the source. (c) Spectrogram of the record, in the frequency window 1.5–6 Hz.

Finally, the exact location and mechanism of the seismic-to-acoustic conversion has to be controlled by the morphology of the shoreline at the depth of the SOFAR channel, on a scale comparable to a few acoustic wavelengths, typically 1 km. For example, the presence of bays, coves or bights at the SOFAR depths will affect strongly and in a different manner the $P \rightarrow T$ and $S \rightarrow T$ conversions. In the absence of its precise knowledge, the combination of all above factors can easily justify $S \rightarrow T$ conversions with stronger amplitudes than $P \rightarrow T$ ones.

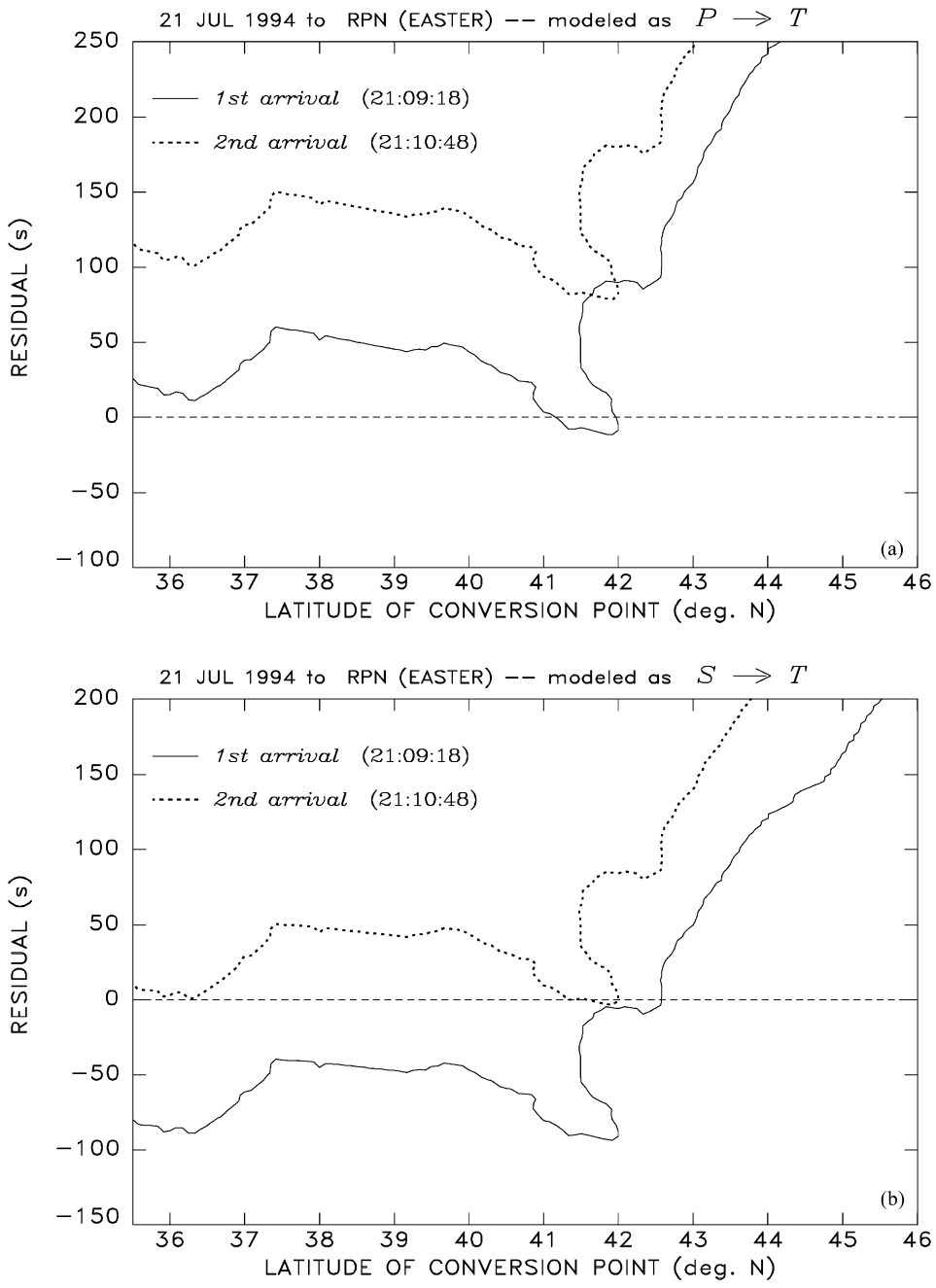

Fig. 2. Residual (observed minus computed) travel-times for the first (solid line) and second (dashes) arrivals at RPN, plotted as a function of the latitude of a hypothetical point of seismic-to-acoustic conversion, on the 1200 m isobath along the Japan–Kuril trench (see Fig. 3). The top frame assumes initial seismic propagation as a *P* wave, the bottom one as an *S* wave.

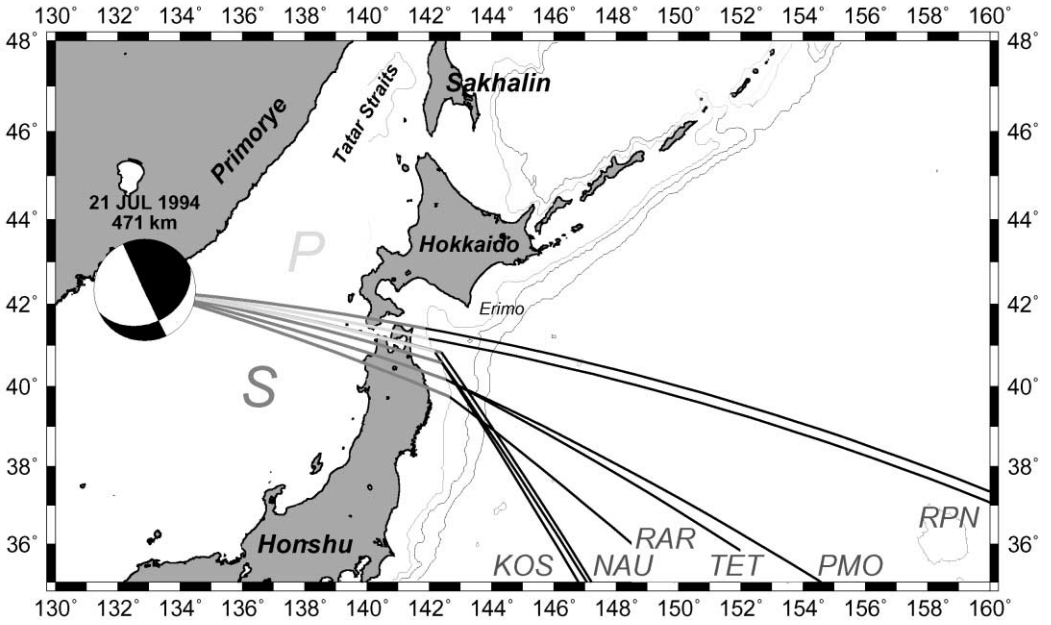

Fig. 3. Map of the epicentral and conversion area for the deep event of 21 July 1994 in Primorye. The seismic paths are plotted as solid (*P*) or dotted (*S*) lines. All arrivals can be explained by conversion of either *P* or *S* to an acoustic wave at the Hokkaido corner.

4. Regional investigations

In this section, we investigate systematically the characteristics of *T* waves generated by deep events in subduction zones characterized by seismicity gaps and/or detached events. We discuss in the main text only the principal events, in particular the so-called "detached" earthquakes. All details regarding additional shocks are given in Appendix A.

4.1. Kuril–Sakhalin subduction zone

In this region, we are of course motivated by the large deep earthquake under Sakhalin on 12 May 1990. The WBZ is well defined to the East, but deep earthquakes were largely undocumented West of 148°E ($h > 600$ km) or 146.5°E ($h > 550$ km). In this respect, the event occurred significantly North of the perceived extent of the WBZ, and was widely described as "isolated" (Lundgren and Giardini, 1994). However, in an independent study involving relocation of historical earthquakes, we have identified a string of hypocenters extending continuously from the Hokkaido corner at (45.5°N, 137°E; 310 km), under the Tatar Straits down to the 1990 Sakhalin event (Okal et al., 1995; Huang et al., 1998).

4.1.1. Sakhalin, 12 May 1990; 49.0°N, 141.8°E; 605 km; $M_0 = 8.2 \times 10^{26}$ dyn cm

We obtained excellent paper records of *T* arrivals in Polynesia. We use stations PMO (Pomariorio, Rangiroa), MEH (Mehetia, Society) and TBI (Tubuai, Austral). Fig. 4 shows the record at PMO. It is obviously characterized by two main arrivals, with maxima at 06:38:12 and 06:39:38 GMT, respectively. No correction is needed at MEH and PMO, since the stations are less than 500 m from the point of acoustic-to-seismic conversion. A 2 s correction was performed at TBI.

Unfortunately, we were unable to find any other record of *T* waves from that event. This is due to several circumstances. In 1990, the demise of the WWSSN was complete, but the IRIS network was not yet operating at full strength, and in particular few broad-band stations were continuously recording, hence no records are available at RAR, RPN,

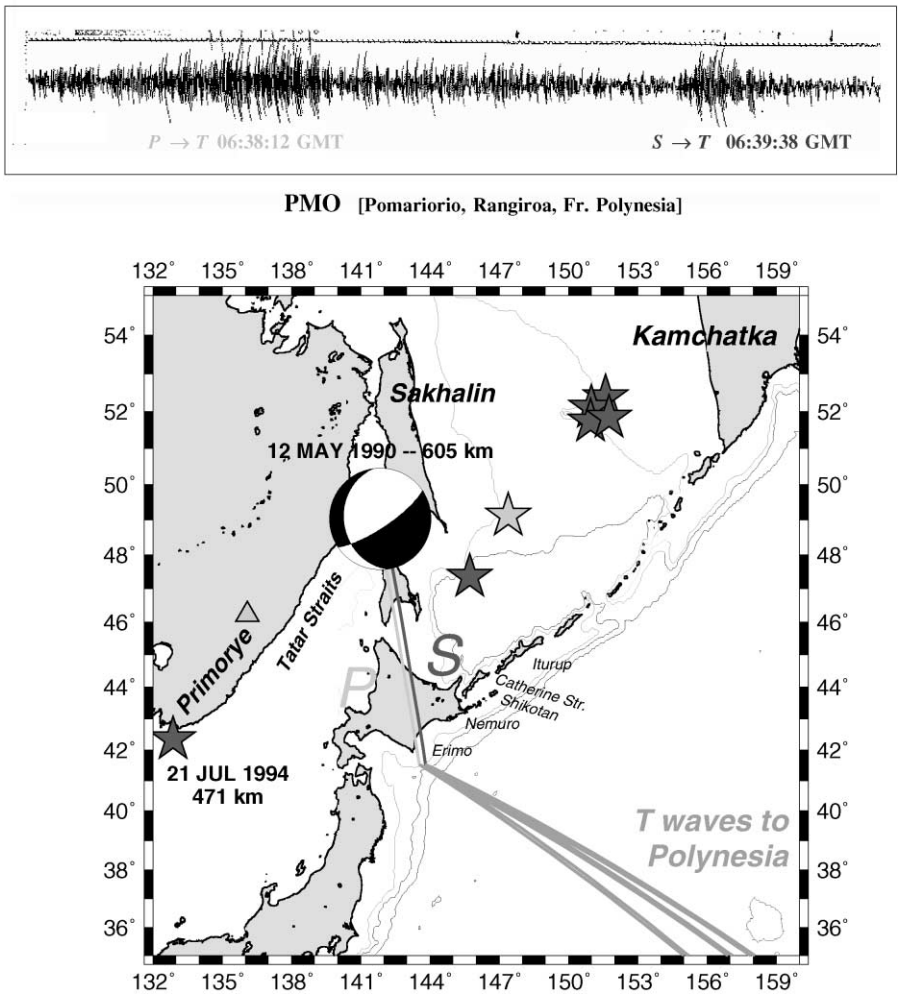

Fig. 4. T waves recorded in Polynesia from the isolated deep earthquake of 12 May 1990. Top: original paper record at PMO. Note the two puffs of high-frequency activity, separated by ∼90 s, which compose the T phase. Bottom: map of the Primorye–Sakhalin–Okhotsk area showing the mechanism of conversion at Cape Erimo, Hokkaido. The stars are other deep events generating T phases into the Pacific Ocean, including the large 1970 Okhotsk Sea earthquake. The event at extreme left is the Primorye earthquake described in Figs. 1–3. The triangle is a small 1997 event at 416 km, confirming the warped geometry of the slab.

AFI. While the broad-band channel at KIP (Kipapa, Hawaii) is continuously available, the station is masked by Kauai, and no T wave arrival could be identified; similarly, a systematic search of the HVO records failed to turn up a T phase. Finally, propagation to California coastal stations is blocked by the Aleutian arc.

Fig. 5 shows that whereas the first arrivals (solid lines) at stations PMO, MEH, and TBI are readily interpreted by a $P \rightarrow T$ conversion, the second maxima in the T waves (dotted lines) occur too late to correspond to conversion from a P wave anywhere along the coastline, from 37 to 50°N (conversion at 42°N; 142°E is not acceptable, because at this location, the offshore direction faces the source rather than the receiver). On the other hand, these arrivals, as well as the maximum in T at TET, are readily explained by $S \rightarrow T$ conversion at the southern tip of Hokkaido,

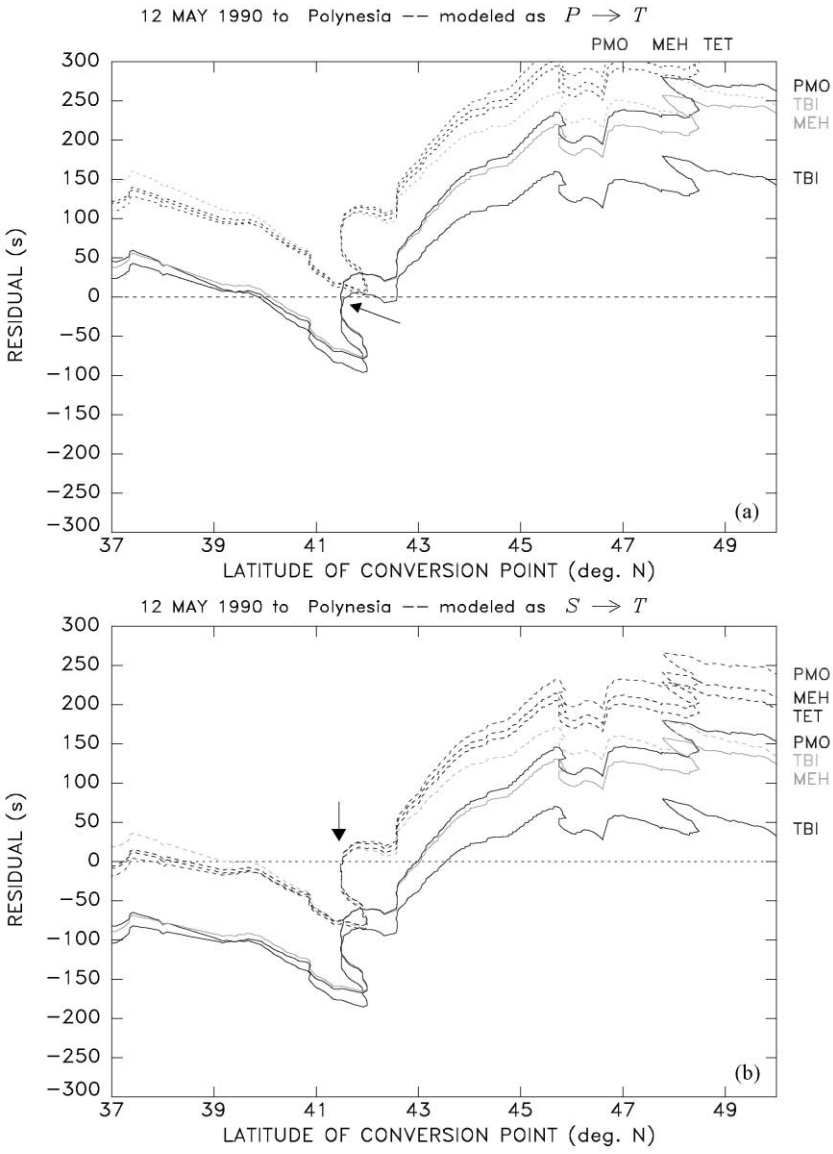

Fig. 5. Same as Fig. 2 for the 1990 Sakhalin event.

in the vicinity of Cape Erimo, at 41.5°N and 143.5°E, essentially the same location as for the $P \rightarrow T$ conversion.

Even though the unavailability of digital data prevents formal spectrogram analysis, the mere propagation of the T wave in the Pacific SOFAR channel requires frequencies of at least 3 Hz, and, thus, our observations indicate the possibility of propagating high-frequency S waves from the Sakhalin deep focus to the Hokkaido corner. We interpret this as evidence for mechanical continuity of the slab in this area.

T waves from additional large deep shocks in the Sea of Okhotsk were studied systematically; all details are given in Appendix A. The emerging pattern is that of the routine generation of T waves from both P and S body waves at the Kuril trench for eastern

Sea of Okhotsk events, and on the southern shores of Hokkaido for the western ones. We note that this conversion is efficient — events as small as 10^{25} dyn cm routinely generate T waves detectable in Polynesia.

In this respect, the 1990 Sakhalin earthquake does not exhibit any singularity in its generation of T waves, as compared with events both in the Sea of Okhotsk to the East (Fig. 1) and in the Sea of Japan to the West (Fig. 3). The slab is vertically mechanically continuous with the lithosphere subducted at the Hokkaido corner, as also documented by the seismic "finger" reaching the 1990 hypocenter (Huang et al., 1998) (we failed to find any new events (1994–1998) which would have updated the seismicity along the finger).

Rather, the northerly position of the 1990 Sakhalin deep shock indicates that the slab is warped, with the subducting angle significantly shallower in the western part of the Sea of Okhotsk than in its eastern part, an interpretation in line with the model of Glennon and Chen (1993), and with the tomographic results of van der Hilst et al. (1991). Finally, it is also borne out by the occurrence of a moderately deep shock under Primorye on 1 October 1997 ($h = 416$ km; $m_b = 5.2$; triangle in Fig. 4), which constrains the WBZ to a northerly location. Faint T waves were recorded from this event at the Wake hydrophones, but were of an amplitude too small for a meaningful study.

4.2. Bonin–Marianas arc

4.2.1. 4 July 1982; 27.9°N, 136.5°E; 552 km; $M_0 = 1.2 \times 10^{26}$ dyn cm

This "isolated" event, mentioned by Okino et al. (1989), was discussed in detail by Lundgren and Giardini (1994). Strong T waves were detected at PMO, where two arrivals are separated by 68 s. No WWSSN or GDSN records could be found for the expected time windows of T waves, but a strong T phase with maximum at 02:34:05 was found at KAA, on the western coast of the Big Island of Hawaii, and a weak but undeniable record is also present at SYP at the western end of the southern California network.

Because the Izu–Mariana arc is composed of discrete island and seamount structures, few of which penetrate the SOFAR channel, the latitude sampling in Fig. 6(c and d) is discontinuous. Even so, the interpretation of the records is somewhat ambiguous. Most arrivals can be interpreted as conversions either at the northern end of the Volcano Islands (Kita Iwo Jima) or at a site on the Bonin Island group. The exception is the SYP record, which can only be interpreted as an $S \rightarrow T$ conversion on Haha Jima, on the southern tip of the Bonin group. Note, however, that the path to SYP involves a 32 s receiver side correction (accounting for 86 km of travel in continental structure), which is bound to be imprecise, given the complex geometry of the shoreline.

The most important observation from Fig. 6(c and d) is that it is impossible to account for the second, stronger arrival at PMO (dotted line in Fig. 6c) by invoking a $P \rightarrow T$ conversion at any of the shallow structures available along the arc. Rather, it is readily interpreted as an $S \rightarrow T$ conversion. Here again, this requires the propagation of strong S waves at frequencies greater than 3 Hz, proving that the slab must be mechanically continuous from the hypocenter to the ocean. The 1982 earthquake cannot have occurred in a detached blob of subducted lithosphere; this result also upholds van der Hilst et al.s' (1991) tomographic section, in which the Bonin slab sags westward above the 670 km discontinuity.

4.2.2. T waves from other events

Other deep events in the Bonin–Mariana WBZ were studied systematically, with full details reported in Appendix A. A remarkable result of this study is that while some travel times can be explained by conversion on the Volcano Islands, none require it; on the other hand, the Wake hydrophone signals (and the possible arrival at SCZ) from the 1996 event (purple star in Fig. 6a) can be explained only by conversion in the Bonin group. In this framework, the latter becomes the only proven scatterer of P and S energy into the SOFAR channel.

This can be understood by noting that unlike the presently active Volcano Islands, the Bonin group is an uplifted fragment of fore-arc basement whose volcanics are at least 40-million year-old, (e.g., Umino, 1985; Taylor et al., 1994). In the fully decoupled Bonin–Mariana subduction zone (Uyeda and Kanamori, 1979), there are few shallow slopes permitting conversion of seismic energy into the SOFAR channel, and in practice, only islands or large seamounts are adequate structures. However, in the geometry of that steeply dipping slab, the seismic rays will arrive vertically to the island and, thus, if the

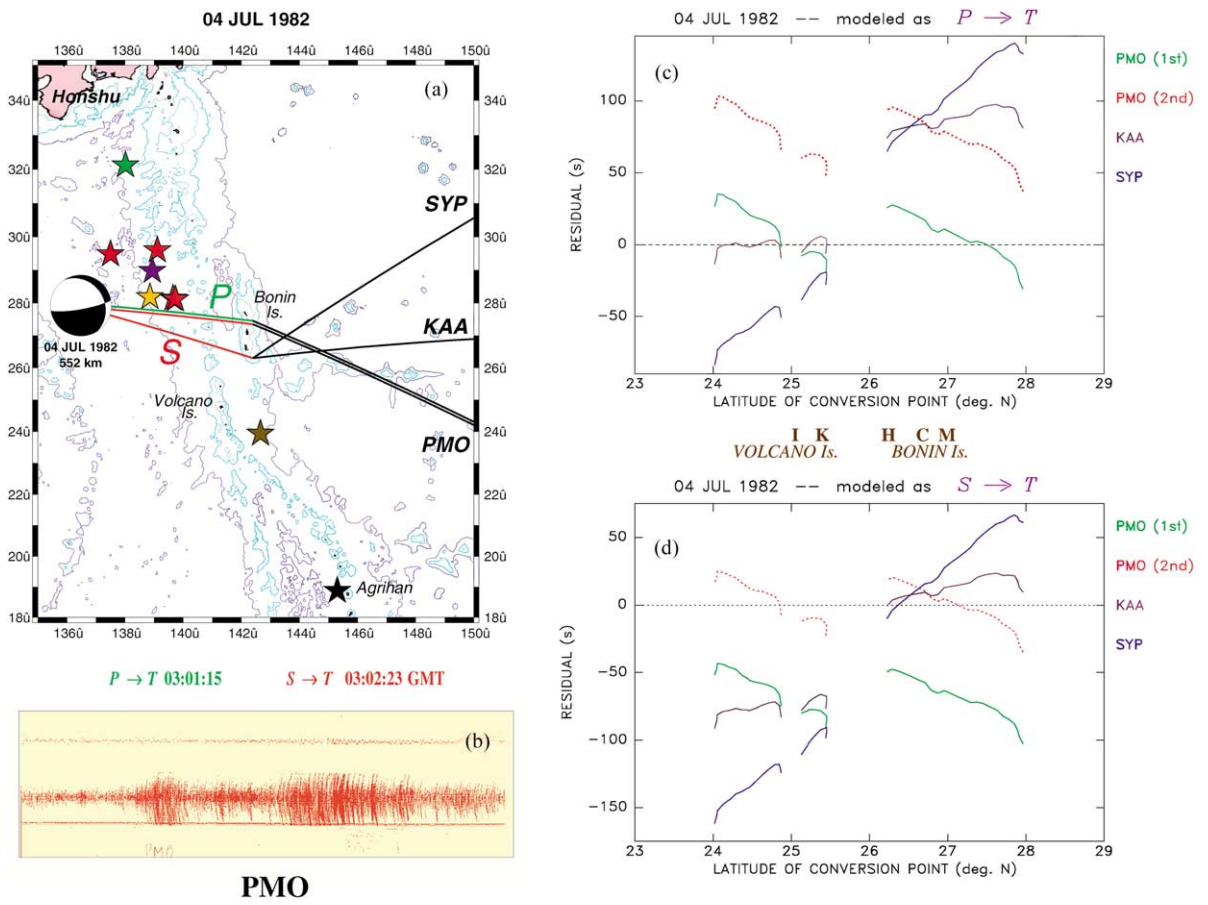

Fig. 6. Composite figure for the 1982 "detached" Bonin earthquake. (a) Location map; ray paths travelled as P waves shown in green, as S waves in red. In addition, red stars show the additional events studied in Appendix A, for which $S \rightarrow T$ phases were observed; other colors are explained in Appendix A. (b) T wavetrain recorded at PMO on the T wave channel. The times of maximum amplitude of the two arrivals are given. (c and d) Modeling as $P \rightarrow T$ and $S \rightarrow T$ conversions. The latitudinal bands of the two island groups are given in brown, with initials indicating the position of the islands mentioned in the text: I, Iwo Jima; K, Kita Iwo Jima; H, Haha Jima; C, Chichi Jima; and M, Muko Jima.

site is volcanic, travel through its magmatic system, characterized by strong anelastic attenuation. As a result, the high frequencies necessary for channeling into the SOFAR will be eradicated, and conversion to an acoustic wave impossible. The Bonin Islands, however, are offset laterally 120 km from the magmatic body under the active arc and have cooled off since 40 million year, to the extent that they can provide a high-Q path from the bottom of the slab to the 1200 m isobath, capable of delivering high-frequency seismic energy into the SOFAR channel. This situation is of course in contrast to more traditional, shallower-dipping and more strongly coupled subduction systems featuring a well-developed fore-arc structure, long known to offer high-Q reception of seismic energy from the bottom of the slab (Utsu, 1971).

We, thus, explain that the Bonin Islands are the only locale along the Bonin–Mariana WBZ capable of efficiently generating T waves from deep earthquakes in a fashion similar to the Kuril shoreline (Section 4.1) or the coast of South America (Paper I and Section 4.3). Note the 1995 shock to the South (black star in Fig. 6a), which did not generate T phases into the

Pacific Basin, despite having the largest seismic moment of the regional group studied, and being in the immediate vicinity of an island (the volcanically active Agrihan). On the contrary, the last event studied, event farther South, did generate a T wave, through conversion on Guam, which is not an active member of a volcanic arc, but rather a limestone-capped uplifted segment of fore-arc basement, estimated to be at least Early Miocene in age (Tracey et al., 1964). Finally, this pattern is also upheld in the Izu region to the North, as documented by the 1993 earthquake, for which conversions are not observed at the nearby volcanic islands and seamounts (e.g. Hachichojima), but rather off the continental structure of southeastern Honshu (see Appendix A).

4.2.3. Other detached events

In the general vicinity of the 1982 shock, we were able to identify two outlying earthquakes, on 23 June 1988 ($m_b = 4.5$) and 12 September 1997 ($m_b = 4.1$), which qualify as "detached" in the sense that they are clearly located in front of the mainstream WBZ (Fig. 7). We relocated these events using the formalism of Wysession et al. (1991). In particular, we attempted unsuccessfully to force the events into the WBZ, by arbitrarily deleting stations. In addition, we performed Monte Carlo relocations after injecting random noise into the dataset, using $\sigma_G = 1.5$ s as the standard deviation of the Gaussian noise, a generous value for such modern events. As shown in Fig. 7b, the resulting error ellipses do not reach the WBZ, and we must conclude that the events are indeed located outside the main body of WBZ.

Another potential candidate, on 9 October 1963, was relocated with its Monte Carlo ellipse reaching the WBZ, and a historical shock on 20 April 1933, listed by the ISS at 20.5°N, 140°E (477 km), is probably an intermediate depth earthquake under the Sea of Okhotsk.

4.2.4. Discussion

We regard the identification of the 1988 and 1997 outliers as a very important result, in that it establishes the continuity of seismogenic material from the WBZ to the 1982 hypocenter. Together with the detection of the $S \rightarrow T$ conversion from the latter, this establishes the mechanical continuity of a segment of slab extending to the location of the 1982 shock. This is in general agreement with regional tomographic models such as Van der Hilst et al.s' (1991) and Fukao et al. (1992), which show a zone of fast P wave velocities extending West of the Bonin arc at the relevant depth (550 km), thus suggesting that the slab sags and stagnates above the lower mantle. This feature is, however, absent from their models for the southern part of the Philippine Basin, West of the Mariana arc. More recently, and based on a comparison between tomographic inversions of P- and S-travel-times, Widiyantoro et al. (1999) have suggested that the stagnating and subducting portions of the Izu–Bonin slab may have different signatures, the latter being unseen in the S tomography. A model compatible with the high-Q path required by our documented $S \rightarrow T$ conversions would have to involve a change of mineralogy increasing the Poisson ratio of the stagnant material, while at the same time keeping a low attenuation.

There is no clear explanation as to why outboard seismicity takes place in front of the WBZ only at the latitude of the 1982 shock and of its two small outlying companions. Of course, the latter observation may be an artifact of a short time sampling of seismological observations. We note the intriguing coincidence of this feature with the presence of the Bonin Islands group to the East, which constitute the only emerged uplifted fore-arc along the whole Izu–Bonin subduction system. One can only speculate that there may exist a common geodynamic agent explaining the apparent upwards deflection of both systems, with obviously very different vertical scales.

4.3. South America

We are motivated in this region by the 1989 earthquake in Paraguay, the third of the main "detached" events reported in the literature (Lundgren and Giardini, 1994).

4.3.1. Paraguay, 28 Feb 1989; 23.11°S, 61.47°W; 569 km; $M_0 = 7.2 \times 10^{25}$ dyn cm

Unfortunately, we were unable to document a consistent set of T waves at Pacific stations which could be associated with this event. There are two T wave signals in Polynesia: a very weak one, legible only on the T wave channel, at RKT (Gambier) at 14:24:47 GMT, the other one at TPT, detectable on the regular

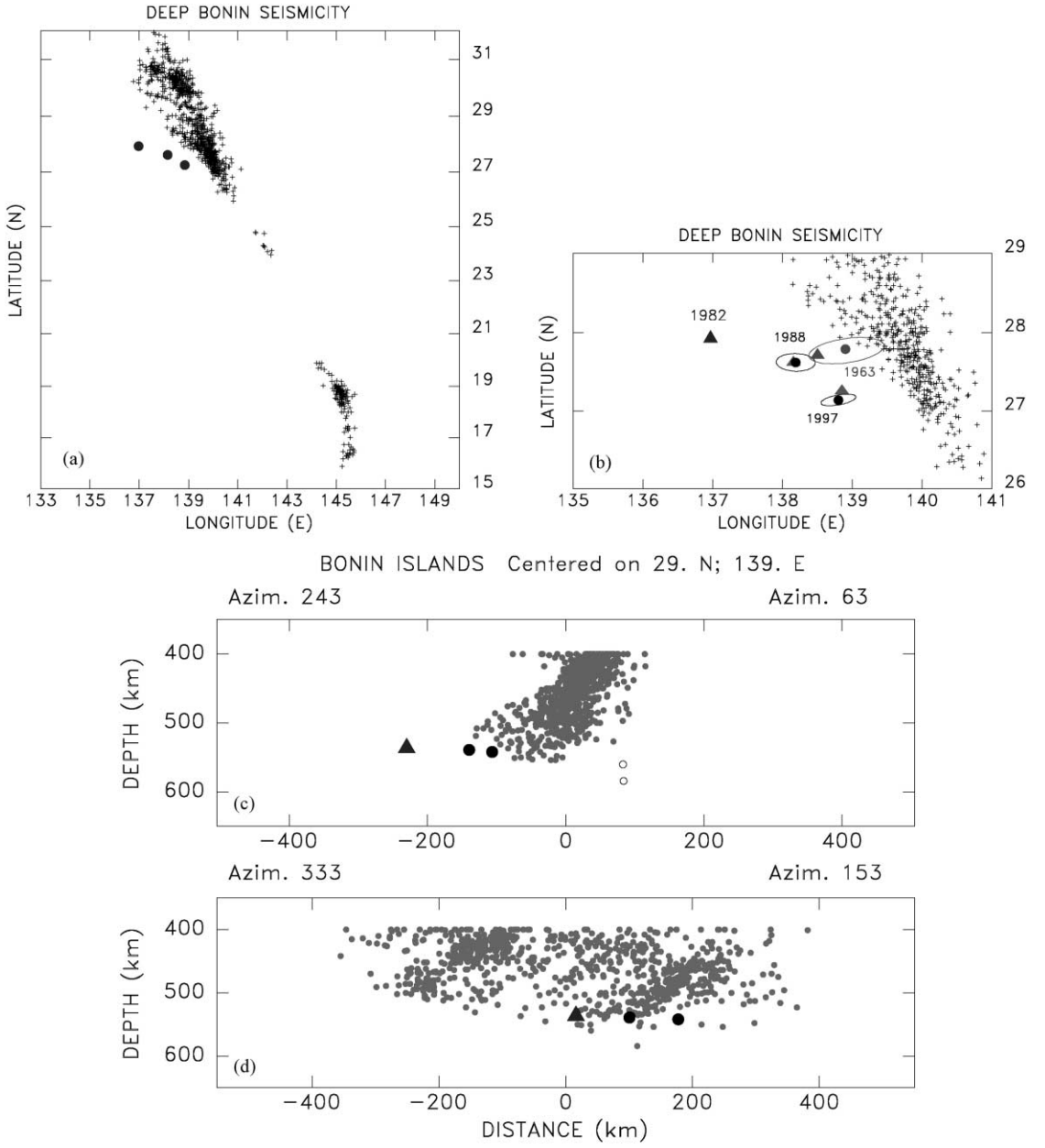

Fig. 7. (a) Deep seismicity of the Izu–Bonin WBZ, showing the three outlying events (1982, 1988 and 1997) as large dots. The '+' signs are unrelocated NEIC earthquakes ($h = 400$ km) for the period 1964–1998. (b) Relocation of the outlying events. The triangles show the original NEIC locations of the 1988 and 1997 events; the dots are our relocations, with associated error ellipses ($\sigma_G = 1.5$ s). Also shown in gray is the 1963 earthquake, listed as outlying in the NEIC catalogue, but relocating to the mainstream WBZ. The ISC estimates of the uncertainty on the 1982 epicenter are $\leq$1.5 km, less than the size of the symbol. (c) Cross-section of the dataset in panel (a) along the azimuth 63°, perpendicular to the strike of the WBZ; only events North of 25°N are included; we verified that the two deepest events, shown as open circles, are poorly located shocks which are not genuine outliers. (d) Cross-section along azimuth 153°, parallel to the strike of the WBZ.

short-period channel at 14:29:19 GMT. These times indicate that the two signals cannot share a common source on the coast of South America. Indeed, they can be reconciled with a small earthquake at 13:19:36 GMT, off the coast of Guerrero, Mexico, a region for which station TPT is particularly sensitive to *T* waves. A systematic examination of both paper and develocorder archives at HVO failed to turn up a legible *T* phase at the coastal station HUL. No IRIS/GDSN digital data are available at appropriate combinations of time windows and sampling rates; similarly we could not find digital *S* wave records at coastal South American stations to investigate the possible presence of high-frequency *S* waves, using the spectral ratio techniques of Paper I.

We conclude that no *T* waves from the 1989 Paraguay earthquake were recorded in the Pacific Basin. Given the adequate performance of the Polynesian stations, and despite the absence of continuous broad-band digital records at that date, we believe that the event did not send measurable *T* phases into the ocean. Noting that its moment is smaller

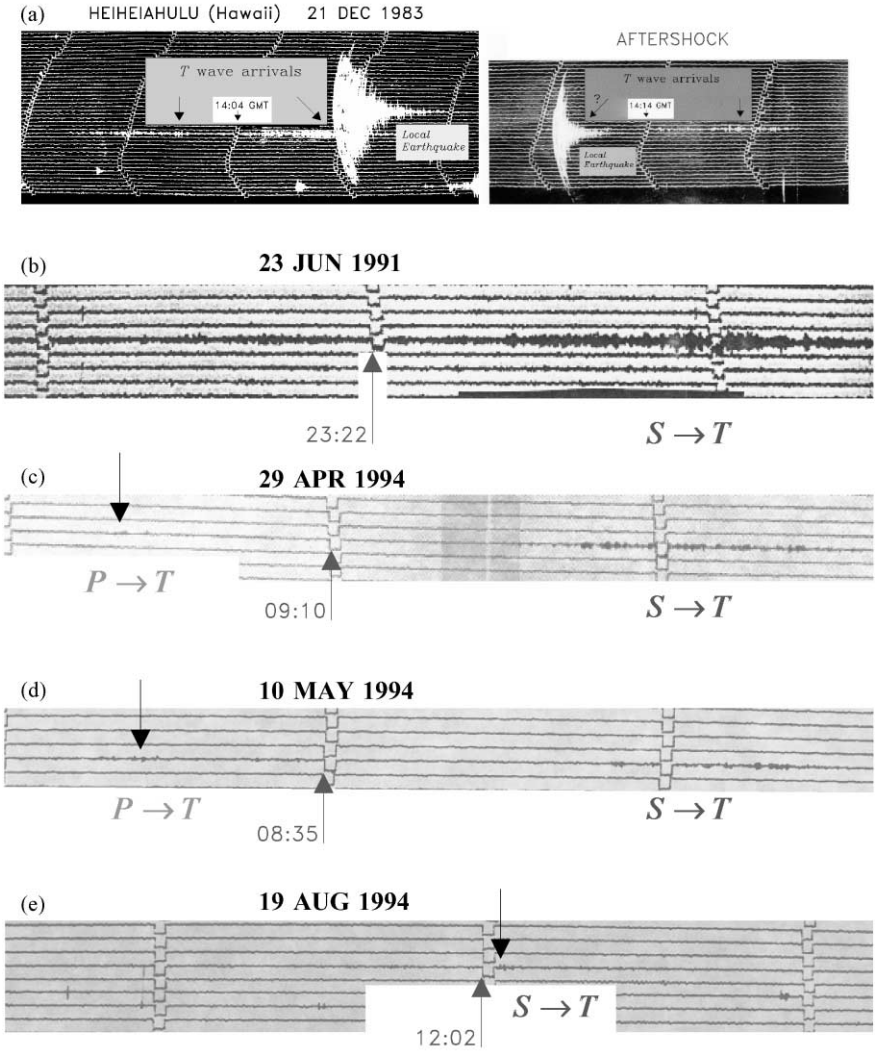

Fig. 8. Comparison of *T* waves received at station HUL from deep events in northern Argentina. This figure illustrates a threshold of $\sim 10^{26}$ dyn cm for their detection.

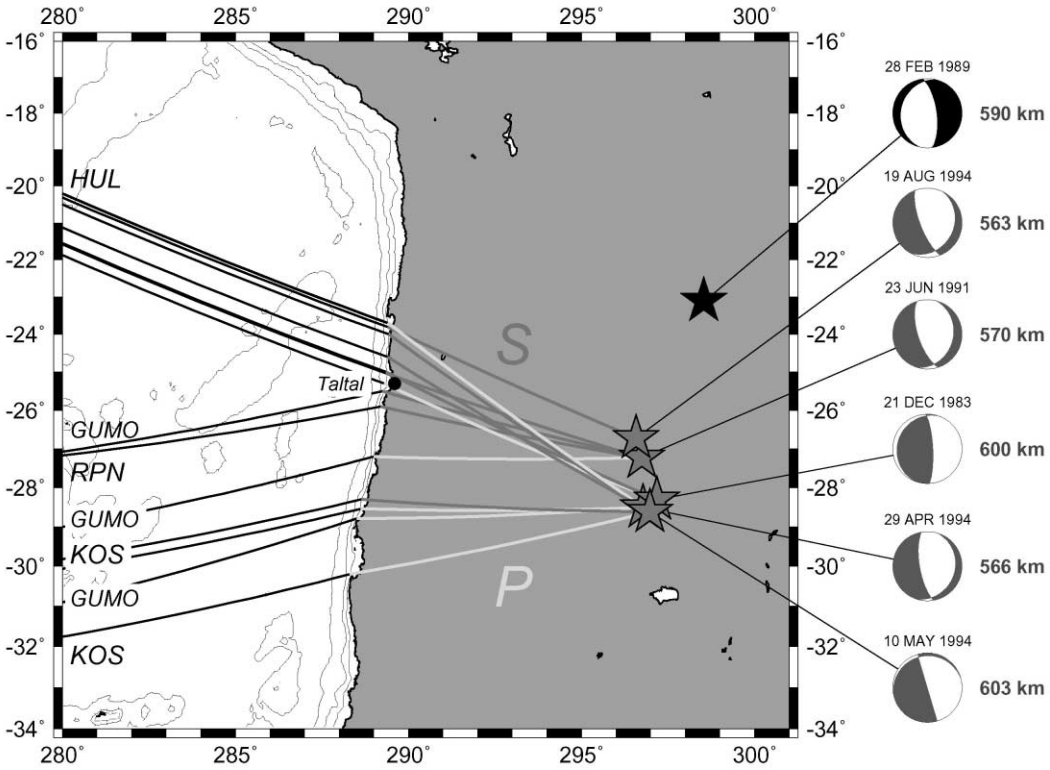

Fig. 9. Map of northern Argentina illustrating the various conversions documented for the events used in the threshold study. The 1989 Paraguay earthquake, for which no T waves were detected, is shown as the black star.

than that of the 1982 Bonin Island and a *fortiori* 1990 Sakhalin "detached" events, we decided to investigate the threshold of detectability of T waves from deep Argentine earthquakes. Specifically, we focus on five events listed in Table 2, and investigate their T waves, primarily at the Hawaiian station HUL. Fig. 8 compares the T waveshapes recorded at HUL, and Fig. 9 verifies that the conversion location is fundamentally similar for all observed T waves. Further details are given in Appendix A. This experiment suggests a threshold of detectability for T waves from deep earthquakes in northern Argentina recorded at HUL of between $M_0 = 2 \times 10^{26}$ and 5.6×10^{25} dyn cm. A practical threshold may then be 10^{26} dyn cm, but unfortunately, no CMT solution exists to fill in the moment gap and refine this estimate. We note that this threshold is significantly higher than in other subduction zones, such as Kuril and Bonin–Mariana.

Of course, the final amplitude of the T wave is controlled in part by a number of unknown factors, such as small scale lateral heterogeneity at the source and conversion point, and high-frequency behavior of the earthquake's source time function, which may not be exactly repeated between events. Thus, an exact correlation between the observability of T waves and seismic moment (or magnitude m_b) would not necessarily be expected. In this sense, our experiment is designed to provide no more than a general order of magnitude of the moment threshold under which T waves from a given region are not expected to emerge from background noise at a given station.

In this context, the absence of T waves from the 1989 Paraguay earthquake may simply express the small size of the event. However, the actual detachment of a blob of seismogenic material cannot be ruled out.

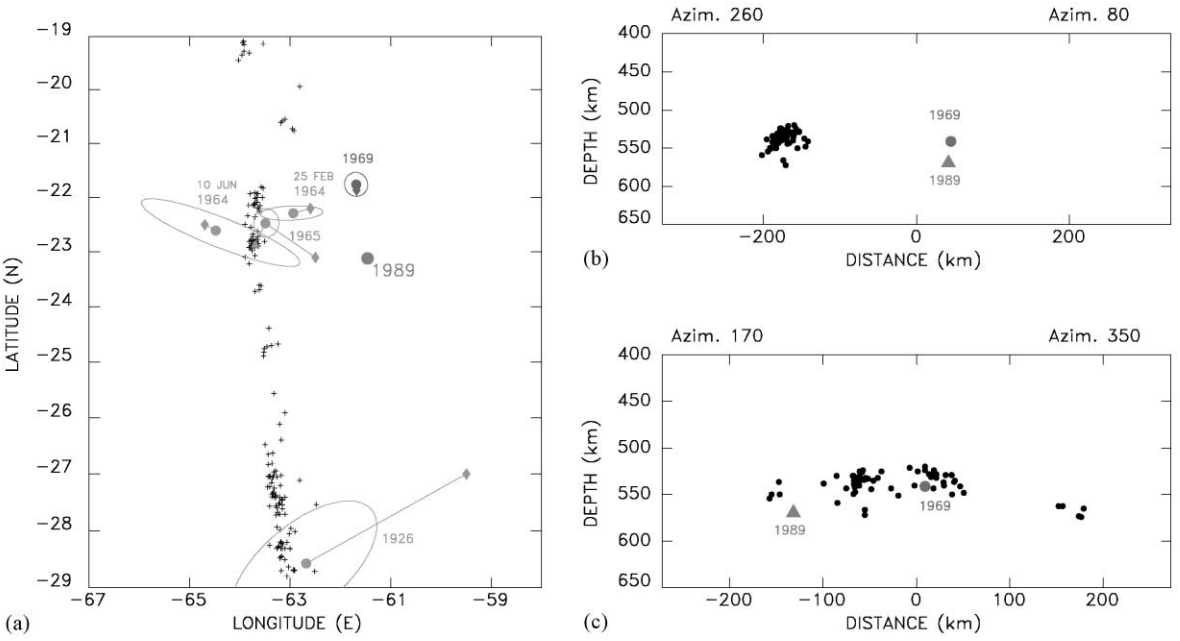

Fig. 10. Outlying deep seismicity in northern Argentina and Paraguay. (a) Map view: the '+' signs are unrelocated NEIC foci ($h \geq 400$ km) for the period 1964–1998. The diamonds identify the original NEIC (or G-R) epicenters of outliers; the inverted triangles are the ISS/ISC locations, when different. The solid dots are our relocations, with error ellipses, as described in detail in Appendix A. The ISC estimates of the uncertainty on 1989 epicenter are ±3.5 km, less than the size of the symbol. (b) Cross-section of the seismicity between latitudes 21 and 24°S, perpendicular to the strike of the WBZ. (c) Cross-section of the seismicity between 20 and 24°S, along the strike of the WBZ.

4.3.2. Other detached events

Again in this region, we investigated systematically the possible existence of additional outboard deep events. The NEIC catalogue (1964–1998) shows three such shocks in the immediate vicinity of the 1989 Paraguay earthquake, on 25 February 1964, 18 February 1965 and 15 April 1969 (Fig. 10). In addition, a historical earthquake in 1926 is given an ISS location 370 km East of the active WBZ, and a lone 1975 earthquake is listed by the NEIC and the ISC 500 km South of the termination of deep seismicity in South America. Finally, a small event on 10 June 1964 is given an "inboard" deep location, West of the WBZ. We relocated all these shocks, using the techniques of Wysession et al. (1991), with all details given in Appendix A. Only the 1969 earthquake is a genuine outboard event. Its final location, 150 km North of the 1989 epicenter, and at a comparable depth (550 km), suggests a similar origin for the two events. The tomographic model of Engdahl et al. (1995) (their Fig. 3f) suggests that around 23°S, the slab sags horizontally before partially penetrating the lower mantle, a behavior not repeated along their "e" profile at 20°S. This could explain that the only known outlying events are at that latitude. The exact mechanism for the distortion of the slab remains unclear. One can simply note (Fig. 10) that the 1989 event takes place ahead of a lateral gap in deep seismicity, which could argue for a local warping of the slab, similar to a curtain fold; this is not the case, however, for the 1969 earthquake.

4.3.3. Bolivia and Colombia

We recall here the study of the 1994 Bolivian deep earthquake in Paper I, which proved that the slab is continuous, both laterally and vertically in that region.

We also refer to Paper I for an analysis of the lone T wave, detected at Reao, from the 1970 Colombian earthquake, which we showed, was generated by a $P \rightarrow T$ conversion along the great circle path from the epicenter. Apart from traces on the analog record at RKT, and despite a systematic search of WWSSN and other databases, we failed to identify T phases

from that event at any other Pacific receiver location. A search for T waves from the small 1997 earthquakes was similarly unsuccessful, so that no definite conclusion can be reached as to the nature of the material separating the three deep hypocenters (1921, 1922, 1970) from the intermediate depth WBZ.

The best argument for mechanical continuity would be the continuous subduction of the Farallon, later Nazca, plate for the past 50 million years; the absence of an $S \rightarrow T$ conversion from the 1970 earthquake can be ascribed to an unfavorable radiation coefficient at the source ($R^{SV} = 0.07$); note also that the P axes for the two historical events are only 16 and 26° away from the one in 1970, and that this common direction would correspond to down-dip compressional stress release in the model of a continuous slab. As for the 1997 earthquakes, they may be simply too small ($m_b \leq 4.8$) to excite detectable T phases. On the other hand, the tomographic results of Engdahl et al. (1995) fail to image the slab through the transition zone, and Grand's (1994) tomographic model is inconclusive.

4.4. Java

The deep seismicity under the Sunda arc has been described in detail by Kirby et al. (1996). Deep earthquakes, absent from Sumatra, are present East of the Sunda Straits at 107°E, but a gap in seismicity exists West of 115°E, between 338 and 470 km. This gap ends significantly shallower than in Argentina. We have verified through relocation (Wysession et al., 1991) the depth of the limiting event (1 June 1997, $h = 470 \pm 17$ km). Based on tomographic studies, Widiyantoro et al. (1997) have proposed necking of the slab under western Java, in a region which would grossly coincide with the seismicity gap. We sought to analyze T waves from deep shocks from this zone; unfortunately, the eastern part of the gap is masked from many sites by Western Australia; in addition, the instrumentation of the Indian Ocean is only very recent, so that we could study only one event, on 19 January 1997.

4.4.1. Java, 19 January 1997; 5.03°S, 108.40°E; 651 km; $M_0 = 1.7 \times 10^{24}$ dyn cm

T wave arrivals could be identified at two stations: Cocos Island and Hope (South Georgia). The records at COCO are characterized by two strong arrivals, which can be interpreted as $P \rightarrow T$ and $S \rightarrow T$ conversions, from a scatterer south of Cape Ujungkulong, at 7.1°S; 105.6°E. This interpretation is, however, non-unique since other points along the coast of Java would also be adequate converters, without the need to invoke $S \rightarrow T$ conversions (Fig. 11). Furthermore, the T waves recorded at COCO are characterized by very low frequencies (down to 1.7 Hz), which should not propagate in a standard Pacific SOFAR channel, but may be explained if the channel is less well defined, i.e. extends over a greater depth range and features faster axial velocities, estimated locally at 1489 m/s (Levitus et al., 1994). Such low frequencies then significantly diminish the power of the method as a proxy for the continuity of high-Q material along the S fragment of the path.

The HOPE record also shows two arrivals, at 04:52:48 and 04:54:51 GMT, the second one being much stronger (Fig. 11(e and f)). Unfortunately, travel-time corrections to Hope are practically impossible to assess given that the 12,700 km great-circle path grazes the Kerguelen Plateau and Antarctica, and samples extreme southern latitudes where the morphology of the SOFAR channel is expected to be strongly altered, with minimum velocities being probably lower but largely uncharted (Levitus et al., 1994). This in turn would suggest off great-circle propagation and quite possibly reflections.

As for the use of spectral properties of S waves, we could not find digital stations in Java sufficiently removed from active volcanic structures to compute a meaningful estimate of Q_μ.

In order to obtain some quantitative assessment of the slab's continuity, we investigated the distribution of deep focal mechanisms both in the zone featuring the seismic gap (West of 115°E) and in the portion with continuous seismicity with depth, defined here as between 115 and 121°E (we do not include mechanisms farther East into the Banda Sea, where the regime of subduction is significantly different). We consider all 47 published CMT solutions deeper than 500 km, including those for 1957–1976 inverted by Huang et al. (1997, 1998), 15 of which belong to the Eastern group, and 32 to the Western one. For each group, we calculate a composite focal mechanism, by summing the moment tensors and solving for the best-fitting double-couple (without weighting the solutions according to moment, which in essence would

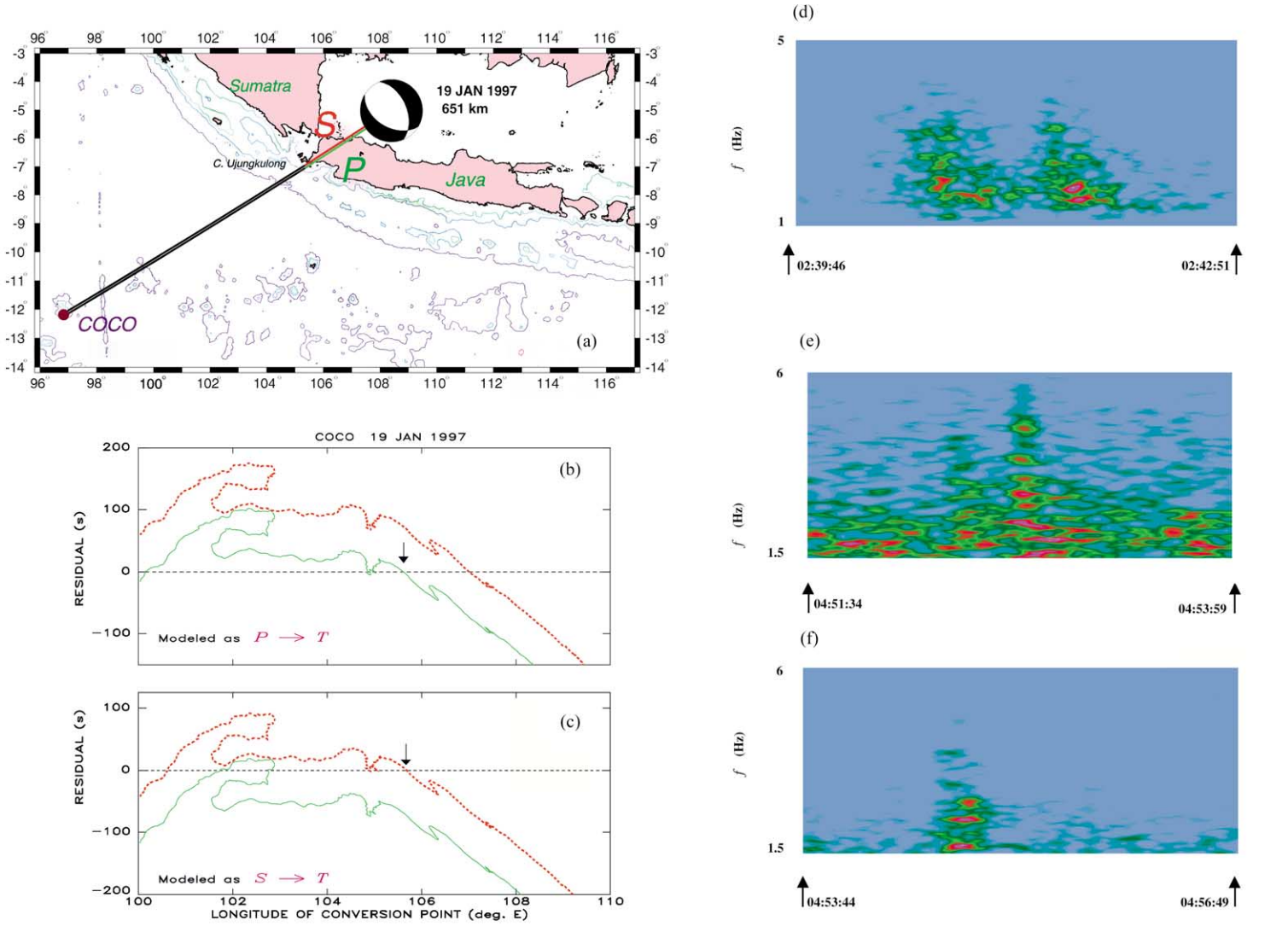

Fig. 11. The deep Java earthquake of 19 January 1997. (a) Map of the proposed paths to Coco Island (COCO). (b and c) Modeling of COCO arrivals as conversions at the Sunda shoreline. (d) Spectrograms of the COCO record. Note the significantly low frequency of the T phase. (e and f) Spectrograms of records obtained at Hope, South Georgia. The scale for spectral amplitudes is 50 times smaller for (e) than for (f).

keep only the contribution of the largest earthquake in the dataset). The results show that the stress release in the Western group remains coherent, and essentially expresses the release of quasi-vertical compressional stress, as it does in the Eastern group. The average *P* axes East and West of the divide dip 85° at azimuth N189°E, and 77° at azimuth N273°E, respectively. These two directions are separated in space by only 13°. Furthermore, the average best double-couples are separated by a rotation of 28° about a steeply (67°) dipping axis, in the formalism of Kagan (1991). This indicates that the predominant down-dip compressional stress believed to control the strain release of the deepest earthquakes is transmitted in a coherent fashion through the seismic gap.

4.5. New Zealand

We investigate here the cluster of deep New Zealand earthquakes, originally discovered by Adams (1963). Table 3 is a list of apparently detached events, updated to June 1999, on the basis of the latest available catalogues. Since the 1998 event has not yet been processed by the ISC, we relocated it based on the dataset available from the EDR files. The essential point is that the depth of the event is perfectly controlled by regional stations, at a value of 600 ± 10 km. Thus, a total of 10 deep New Zealand earthquakes are now confirmed from teleseismic records. None of the six recent shocks were large enough to be processed by the Harvard CMT project, and so, no modern focal mechanism is available. Adams (1963) proposed a thrust mechanism for the 1960 event, based on world-wide first motion readings. Fig. 12 shows a map view and a cross-section along strike of the relevant seismicity.

T waves are routinely recorded from those and other deep Kermadec events at Pacific stations, such as TBI, PPT, RPN, and even KIP, often showing complex wavetrains, suggesting multipathing. However, the interpretation of their arrival times is made difficult, if not outright impossible, by the presence of numerous shallow structures, including the Chatham Rise, which provide a large selection of potential converters. Consequently, the identification of possible $S \rightarrow T$ converted phases at distant receivers is not a realistic means of investigating the structure of the slab.

Rather, we use here the spectral ratio technique described in Paper I, based on three-component broad-band data at station South Kariro (SNZO). IRIS records are only available for the three events of 8 July 1992, 8 April 1994 and 4 July 1998. The records of the small event of 1992 have poor signal-to-noise ratios, and only the other two events could be studied (Figs. 13 and 14). Over the exact same frequency range (1–3 Hz), we obtain an average estimate of $Q_\mu = 300$, which is very significantly lower than found in Paper I for Bolivia–northern Chile, where a continuous path had been documented by $S \rightarrow T$ conversions. By contrast with this situation, we surmise that the path from the deep seismic cluster to SNZO is not made of continuous cold-slab material. This value of Q_μ is only an estimate, but we note that the results for the two events are surprisingly consistent, despite different waveshapes, suggestive of different focal geometries. We propose that this value represents a weighted average of Q_μ^{-1} along

Table 3
Deep earthquakes under New Zealand

Date (D M (J) Y)	Origin time (GMT)	Epicenter		Depth (km)	Magnitude	Reference
		°N	°E			
24 MAR (083) 1953	03:37:13.0	−38.9	174.5	570	5 M_L	Adams (1963)
23 MAR (083) 1960	01:32:18.0	−39.05	174.87	607	6.25 M_L	Adams (1963)
23 MAR (083) 1960	01:36:35.7	−39.10	175.07	612	6.2 M_L	Adams (1963)
7 FEB (038) 1975	15:19:43.0	−39.27	174.26	582	4.9 M_L	Adams and Ferris (1976)
14 SEP (257) 1991	14:14:42.0	−39.180	174.434	602	5.0 m_b	ISC on line Bulletin
26 FEB (057) 1992	00:05:33.7	−38.896	174.693	602	4.0 m_b	ISC on line Bulletin
8 JUL (190) 1992	12:25:25.0	−39.116	174.362	622	4.9 M_L	ISC on line Bulletin
5 MAY (125) 1993	03:51:19.2	−38.903	174.440	577	4.6 M_L	ISC on line Bulletin
8 APR (098) 1994	04:06:54.8	−39.194	174.455	602	3.8 m_b	ISC on line Bulletin
4 JUL (185) 1998	07:47:47.5	−39.16	174.510	600	4.3 m_b	This study

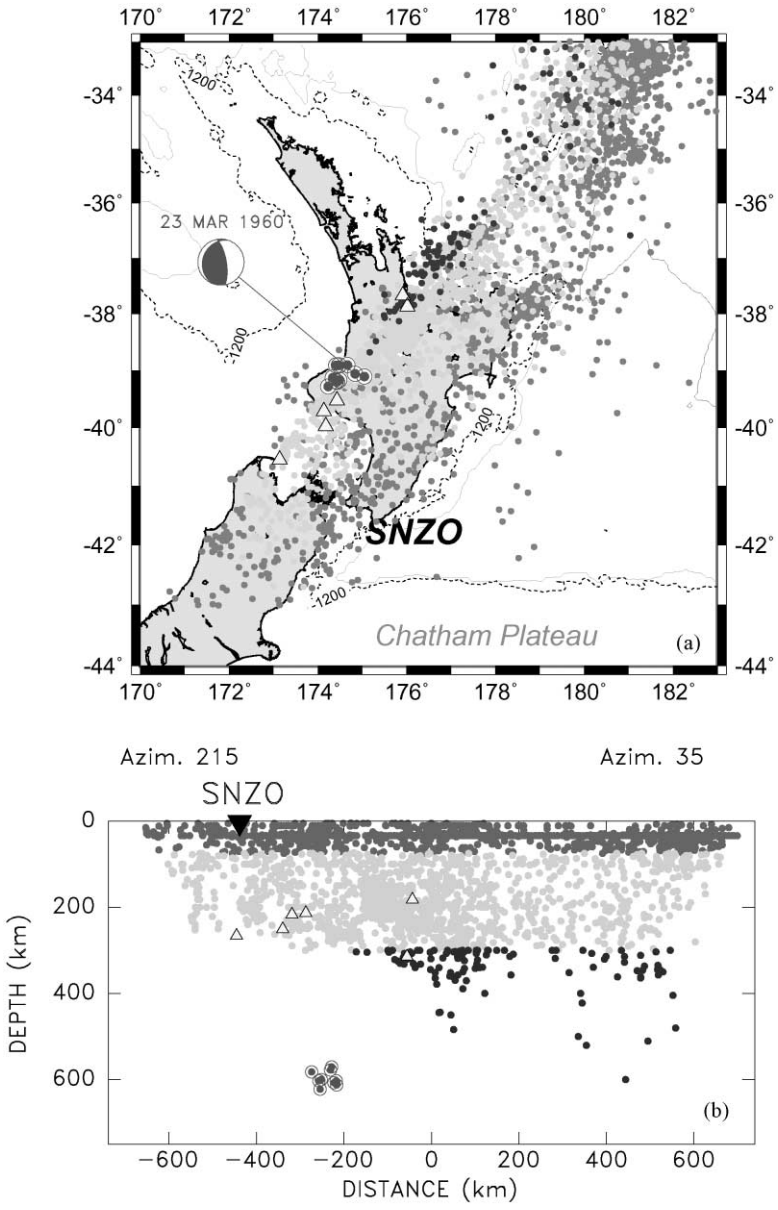

Fig. 12. (a) Map of New Zealand seismicity emphasizing the deep cluster. The events are coded according to depth ($h \leq 75$ km: small, light gray dots; $75 < h \leq 300$ km: medium gray dots; $h > 300$ km: black dots). The deep events listed in Table 3 are shown as larger bull's eye symbols. Focal mechanism is after Adams (1963). The triangles are shallower events also investigated. (b) Along-strike cross-section of the seismicity. Both frames use unrelocated NEIC hypocenters.

a path composed of one-third cold, seismogenic, slab (∼200 km with $Q_\mu \approx 800$), and two-thirds background mantle (∼400 km with $Q_\mu \approx 250$, a possible value for the bottom of the transition zone (Okal and Jo, 1990)), all these numbers being tentative.

Finally, we note that Adams and Ferris (1976) had proposed the identification of a possible structural

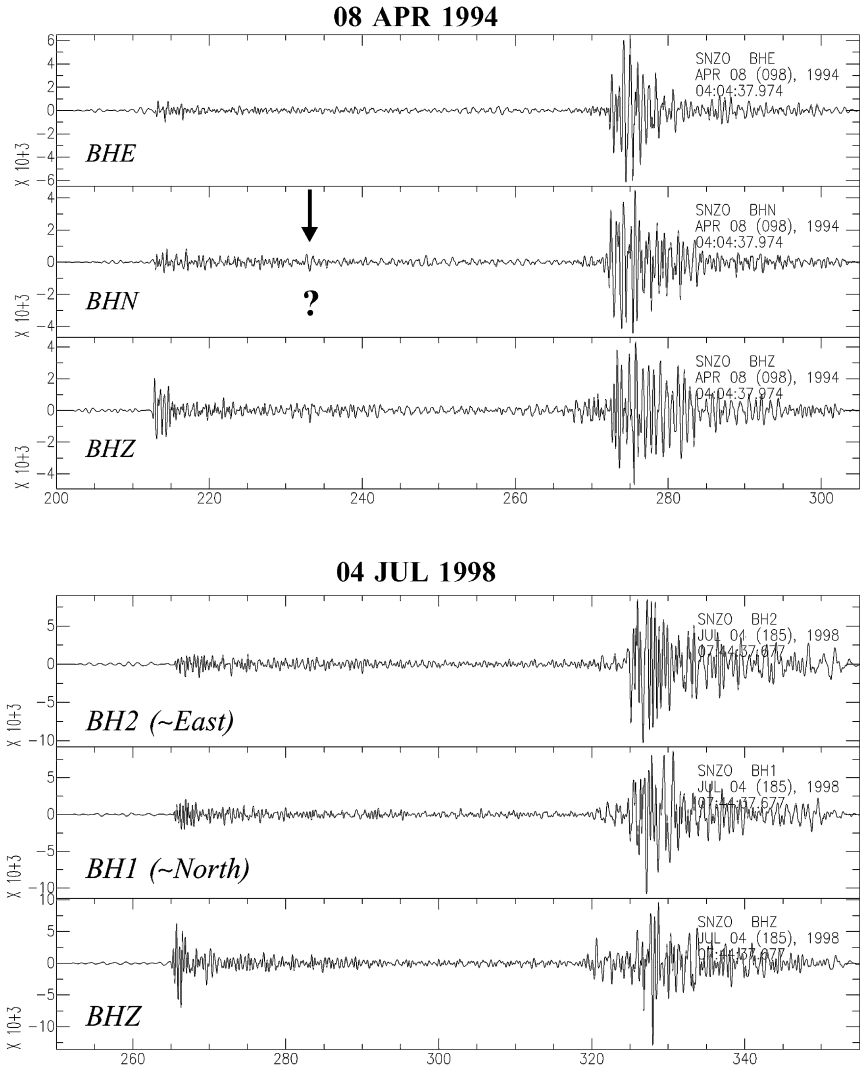

Fig. 13. Three-component *P* and *S* waveshapes at South Karori (SNZO) for the two deep New Zealand earthquakes of 8 April 1994 (top) and 4 July 1998 (bottom). For the former, the arrow identifies a possible converted phase, similar to those discussed by Adams and Ferris (1976).

transition, based on intermediate arrivals observed between *P* and *S* at New Zealand stations from events in the deep cluster, which they interpreted as $P \rightarrow S$ conversions. Fig. 13 shows that such an arrival may be present on the SNZO record of the 1994 event. Being most prominent on the NS component (naturally polarized as SV), it could represent a $P \rightarrow S$ conversion, in contrast to the $S \rightarrow P$ phase claimed by Adams and Ferris (1976). Its timing, 20 s after *P*, would correspond to conversion two-third of the way to the station, or at ∼200 km, which is approximately the local depth extent of mainstream seismicity. This interpretation is, however, non-unique since the conversion could for example occur as part of an internal reflection inside a mechanically continuous slab. Indeed, we have found arrivals intermediate

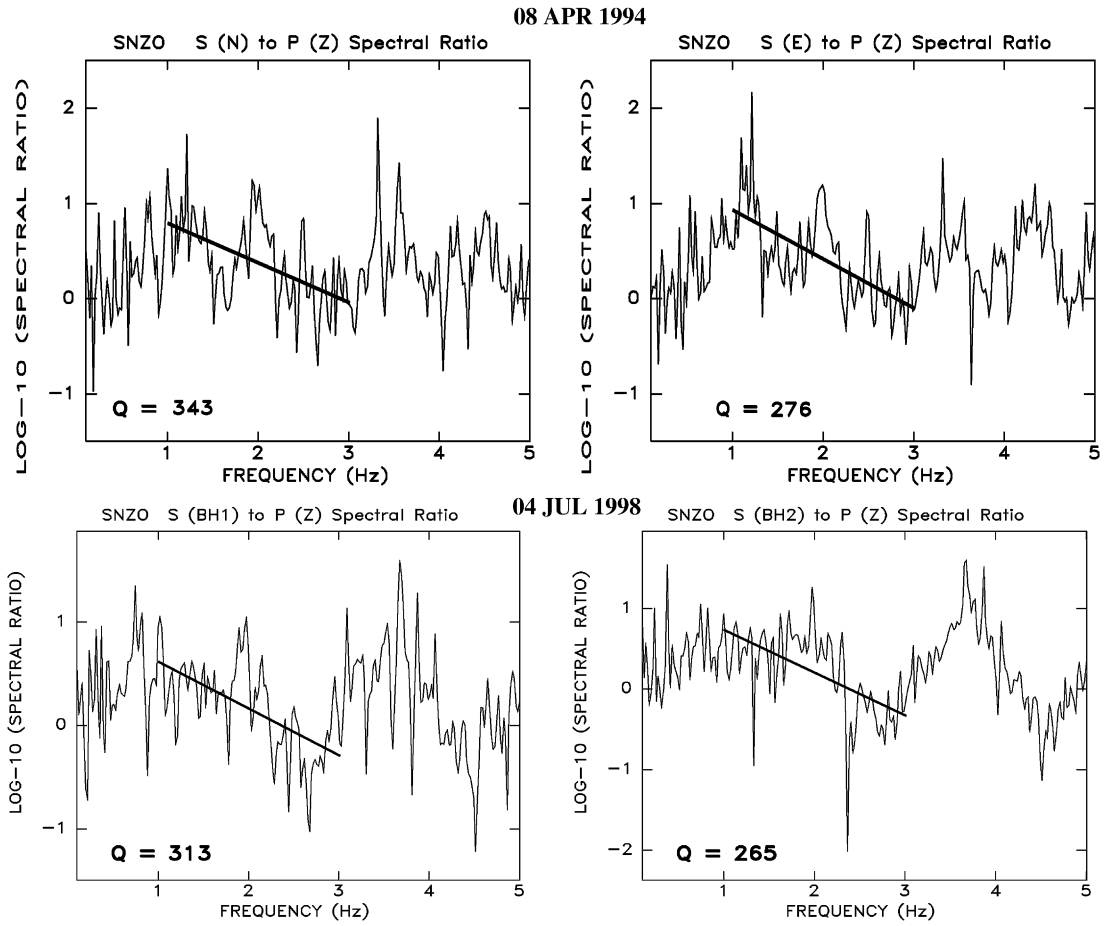

Fig. 14. Estimation of Q_μ on the quasi-vertical path from the New Zealand deep shocks to station SNZO. Each figure shows the variation of the spectral ratio $X_S(\omega)/X_P(\omega)$, for two events and two sets of components: at left North–South (essentially SV); at right East–West (SH). The straight segments provide the regressed best linear fit to the logarithmic decay of the ratio with frequency between 1 and 3 Hz.

between P and S on vertical records at SNZO of shallower, mainstream events (shown as triangles in Fig. 12). Such phases would more precisely match the description given in Adams and Ferris (1976), but would violate their model because of the continuity of the slab to those shallow sources. Finally, the $P \rightarrow S$ conversion reported here is absent for the 1998 event, but this could be due to a different focal mechanism.

To a large extent, the body of data available from the few and small deep New Zealand earthquakes is still inconclusive. However, the following arguments would favor a mechanical separation between the deep cluster and the mainstream WBZ: the relatively low value of Q on the near-vertical path to SNZO, the tentative $P \rightarrow S$ converted phase on the 1994 record, and the down-dip tensional character of the mechanism ($\phi = 350^\circ$; $\delta = 71^\circ$; $\lambda = 79^\circ$) determined by Adams (1963) for the 1960 earthquake. In particular, the first two observations are generally consistent with the mechanical termination of the slab at the depth of cessation of mainstream seismicity. Finally, we note that the tomographic results of van der Hilst and Snieder (1996) would suggest the existence of a body of slow wavespeed between depths of 250 and 500 km at 40°S (their Fig. 12e).

4.6. Vityaz

The Vityaz deep cluster, under the North Fiji Basin, was studied in detail by Okal and Kirby (1998). Since this study was completed, 34 more deep earthquakes (spanning July 1996–June 1999) have been given preliminary locations in the cluster. While the precise depths of these events have not been determined, their epicenters generally fit the several groups identified by Okal and Kirby (1998); the two available new CMT solutions are of small moment (1×10^{24} and 2×10^{24} dyn cm); one mechanism is normal faulting, the other strike-slip. Finally, an intermediate shock given at 200 km under the North Fiji Basin, on 14 November 1997, is most probably a shallow crustal earthquake in the North Fiji Basin: the dataset of 10 stations is found to have no depth resolution.

Despite the availability of good records at KIP, PET, GUMO, SNCC and TKK, we failed to identify *T* phases from the largest recent deep Vityaz event, on 13 April 1995. This suggests that high-frequency energy is not transmitted to the earth's surface North of the Vityaz trench, where adequate converters would exist in the form of numerous shallow bathymetric structures. This supports Okal and Kirby's (1998) conclusion, namely that the Vityaz seismic cluster resides in a severed piece of lithospheric slab, orphaned from the Pacific plate after the reorganization of subduction along the Tonga and Vanuatu systems, and having lain recumbent at the bottom of the transition zone ever since.

4.7. Spain

In this relatively complex tectonic province, the main unanswered question remains the origin of the deep seismicity. Any integrated tectonic model should also explain a growing body of geophysical data at shallower depths, in particular intermediate depth seismicity.

A large scale tomographic experiment by Blanco and Spakman (1993) has imaged a possibly continuous slab, extending in a generally SW–NE direction, between depths of 200 and 670 km. Its structure, with *P* wavespeed anomalies of +1.5%, would be compatible with subduction of oceanic lithosphere, and its size much larger than the 100 km scale, which Grimison and Chen (1986) argued was the maximum width of a paleo-ocean separating Europe and Africa from which to drain such material. Blanco and Spakman (1993) also note that the mapped anomaly does not extend to the surface, and thus speculate that the imaged slab may have been detached, possibly as early as the Miocene, whereas Grimison and Chen (1986) suggest sinking over only a few million years.

The focal mechanism of the 1954 earthquake was worked out by Chung and Kanamori (1976), Udías et al. (1976) and Buforn et al. (1991). Their solutions are generally similar, with the azimuth of dip of the *P* axis varying from N87°E to N61°E, only in fair agreement with a down-dip compression in the geometry of Blanco and Spakman (1993), which would require a more southerly azimuth. The small events of 1973 and 1990 were also worked out by Buforn et al. (1991, 1997), who found mechanisms close, but not exactly similar, to that in 1954.

At shallower depths, we refer to the recent relocations by Seber et al. (1996) and Mezcua and Rueda (1997), who mapped the main body of intermediate depth seismicity as spanning a 140 km long segment oriented N10°E across the Sea of Alborán, from Spain to the northern coast of Morocco. This places its northern end 50 km southeast of the epicenters of the deep shocks (Fig. 15a). Seber et al. (1996) also document strong seismic attenuation in a lower crust–upper mantle body extending at depths of 20–60 km under the Sea of Alborán, and underlain by a more rigid and seismically active mantle structure which they interpret as a fragment of continental (Spanish) lithosphere, delaminated below asthenospheric material under the Sea, that they relate to Neogene volcanism in the Sea of Alborán (Bellon, 1981). On the other hand, Lonergan and White (1997) question the generation of melt in this geometry, and Morales et al. (1999) present a model supported by local *P* and *S* wave nseismic tomography and gravity data, suggesting active continental subduction under the Sea of Alborán.

In this general framework, the question remains of the exact source of seismogenic material for the deep Spanish earthquakes, of its history, and of its relationship, if any, to the subducting or delaminating segments carrying the present intermediate seismicity. It should be emphasized that the relative geographical offset between the intermediate and deep seismicity is not compatible with a single subducting structure along the geometry outlined by Blanco and Spak-

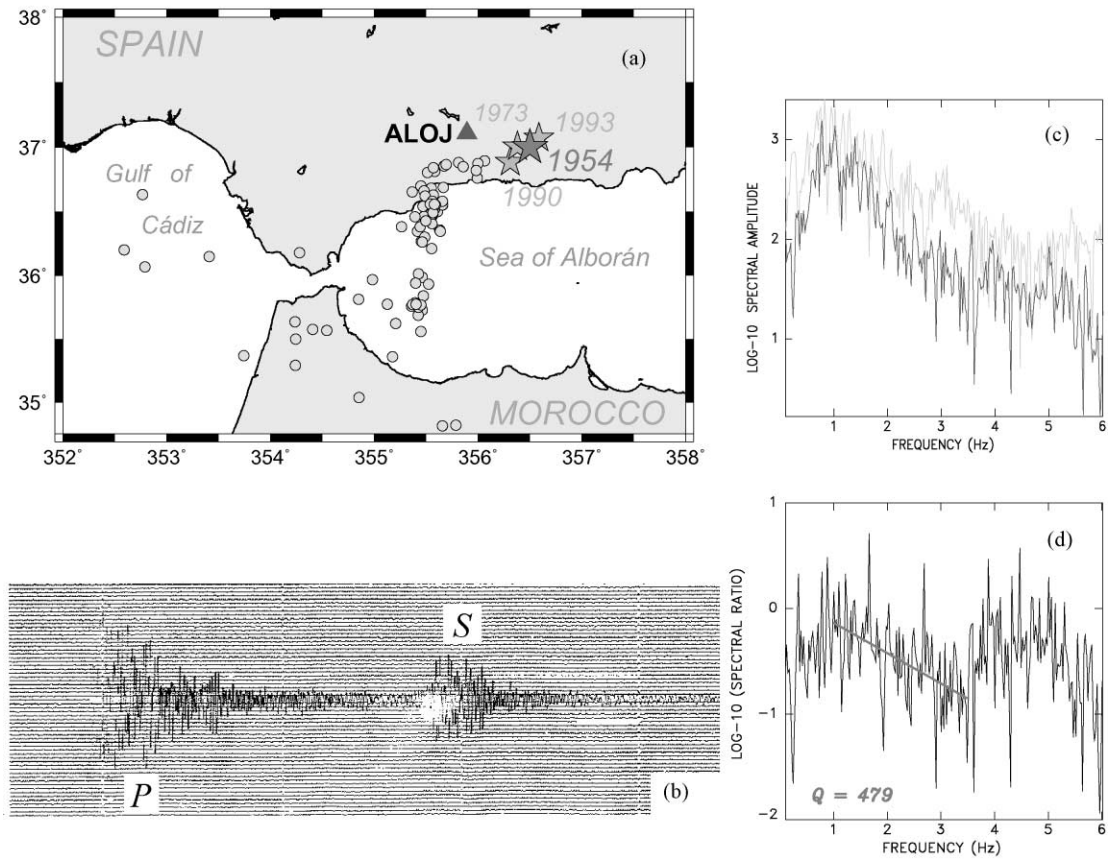

Fig. 15. (a) Map of southern Spain and northern Morocco, showing the epicenters of the deep Spanish earthquakes (black star: 1954 event; white stars: subsequent smaller shocks). The solid dots are unrelocated NEIC epicenters of intermediate depth earthquakes ($h \leq 70$ km) for the period 1964–1998. Also shown (triangle) is station ALOJ used in the attenuation analysis. (b) Original analog record at ALOJ of the deep shock of 8 March 1990 (courtesy of Dr. J. Morales); tick marks are minutes. The epicentral distance is 44 km, and the focal depth 637 km. (c) Spectral amplitude of the P (gray) and S (black) wavetrains obtained after hand-digitizing (b). (d) P-to-S spectral ratio at ALOJ, used to estimate Q_μ between 1 and 3 Hz.

man (1993); rather, such an association would require subduction with a strike of ∼N10°E, which would be more in line with the suggestion (Royden, 1993; Lonergan and White, 1997) of the westward rollback of a short eastward-dipping subduction zone. In such a geometry, a cold slab continuous from the deep foci to the surface could provide efficient channeling of high frequency energy, with the possibility of a conversion into T waves at the eastern shores of the Gulf of Cádiz. We therefore attempted to identify T phases received from the deep Spanish events.

We could not find any T phase records from any of the four deep Spanish shocks. The dataset inspected included the 1954 short-period record at Bermuda, the available WWSSN collection of Atlantic stations for the 1973 earthquake, and all available IRIS time series for the 1990 and 1993 earthquakes.

This negative search remains, however, inconclusive, given on the one hand the low quality of instrumentation for the large 1954 shock, and on the other hand the extremely small size ($m_b \leq 4.1$) of the more recent earthquakes.

We then studied spectral amplitude ratios for a vertical path from the deep 1990 event to a station in Andalucía. An analog record adequate for hand-digitizing and processing was obtained at station

ALOJ, for which the quasi-vertical path would be expected to sample the structure imaged by Blanco and Spakman (1993). We obtain $Q_\mu = 479$, a value intermediate between that of a typical upper mantle average (200) and the much higher values (800–1000) characteristic of propagation through actively subducting cold slabs (Paper I; Mele, 1998). Being higher than the typical mantle average, it requires sustained propagation through cold material, and also a path avoiding the asthenosphere. A tentative model involving a 440 km path in (Blanco and Spakman, 1993) structure, assumed to have $Q_\mu = 700$ (this lower value reflecting possible reheating after detachment), would require $Q_\mu = 283$ for the complementary segment from 200 km depth to the surface, which incidentally samples the zone of intermediate depth seismicity, and remains significantly North of the attenuating body, as mapped in Fig. 2 of Seber et al. (1996). The estimate $Q_\mu = 283$ would be in the range of values for continental lithosphere, given in particular the uncertainty on the thermal structure of a subducted or delaminated fragment (Mitchell, 1995).

It is clear that these results remain very tentative, and that further experimentation, hopefully with digital data acquired during future deep Spanish earthquakes, is warranted.

5. Conclusion

Having examined in detail "detached" or isolated deep earthquakes in eight different environments, we can draw the following conclusions.

1. T phases are routinely generated by the deepest earthquakes, as documented for example in our studies of the Sea of Okhotsk, northern Argentina or the Izu–Bonin systems. The threshold of detection at teleseismic distances varies significantly with the relevant subduction zone; we have found it to be particularly low in Java and much higher in South America. This variation is probably related to the morphology of the converting slope for each subduction zone.
2. In two cases out of three (Sakhalin and Bonin) of detached earthquakes occurring outboard of well-documented WBZs with abundant seismicity, we offer proof of mechanical continuity with the subducting slab. The evidence includes $S \rightarrow T$ conversions, and a string of seismic activity at lower magnitudes. In the third case (Paraguay), we fail to document T phases, but we take note that the earthquake falls below the threshold of detectability from nearby deep shocks; we document an even smaller outboard event 145 km to the North. In general, our results are also compatible with tomographic images, and suggest that the slab undergoes warping, resulting in an offset of the seismicity, rather than tearing and detachment of a lump. In Sakhalin, this is probably related to the cusp in subduction at the Hokkaido corner; in Bonin, we can only make the intriguing observation that the fold in the slab seems to correlate geographically with the presence of the uplifted Bonin Islands at the same latitude along the subduction zone. In Paraguay, we can offer no insight into the mechanism of warping.
3. In subduction zones where a depth gap in seismicity is observed, the presence of $S \rightarrow T$ conversions proves that the slab is indeed mechanically continuous through the gap, the latter expressing only a change in the seismogenic character of the material, rather than the physical separation of a deep blob. In Argentina and Bolivia, this is upheld by the consistency of focal mechanisms, and by tomographic imaging. The temporary loss of seismogenic potential (between 337 and 502 km in Argentina) can be ascribed to an age discontinuity in the subducting material, in the model of Engebretson and Kirby (1992). In Java, where tomography suggests necking of the slab, our T wave results support a continuous slab, without requiring it, the best evidence for mechanical continuity being the coherence of focal mechanisms for the deep events below the gap.
4. The cases of Colombia and Spain are somewhat comparable regarding the extreme isolation of the seismicity, mostly expressed by very large shocks, but differ in relation to small events, present in Spain at the same location as the large ones, but apparently offset to the South in Colombia. Also, Colombia is part of a well-documented major subducting system, whereas Spain is not; on the other hand, a large fast slab is imaged by tomography under Spain, but is not detected under Colombia. In both cases, an argument can be made for

mechanical continuity based on the geometry of stress release: Bina (1997) has modeled downward compressional stresses at the bottom of sinking slabs from the integral of buoyancy forces resulting from the retardation of phase transformations in the cold interior of slabs. A continuous slab, extending several hundred kilometers up from the seismic foci, would provide a consistent domain over which these forces can be integrated in a coherent fashion, whereas a small blob extending only 100 km or less around the seismogenic zone, would not. Thus, it is probable that both Colombia and Spain have a mechanically and thermally continuous slab, since they both feature consistent down-dip compressional stresses. Additional evidence supporting this model exists but its nature is different: in Spain, it comes from tomography and high Q values; in Colombia, mainly from the history of subduction of the Pacific lithosphere and from the geometry of stress release. Both interpretations leave substantial questions unanswered: in Spain, the origin of the material, as discussed by Grimison and Chen (1986), and the orientation of the stress with respect to the slab imaged by tomography; in Colombia, the absence of any detectable tomographic signal, and of low-level seismicity around the 1970 focus (Okal and Bina, 1994, 2001).

5. On the other hand, the Vityaz cluster, where abundant seismicity occurs at relatively low moment levels, and with incoherent geometries of stress release, is most easily explained as a severed piece of lithosphere lying recumbent on the top of the lower mantle, as proposed by Okal and Kirby (1998). The failure to detect any T waves from these deep earthquakes would support this model, but a major difficulty resides in the thermal state of the severed fragment which is expected to be cooling too fast to preserve metastable olivine as a candidate seismogenic material (Van Ark et al., 1999).
6. This leaves the case of the deep New Zealand earthquakes as perhaps the most intriguing and enigmatic detached events. The extreme complexity of the local coastlines makes it impossible to interpret their T waves. A significant body of evidence consisting of the lone available focal mechanism, tomographic results, relatively low Q values, and the tentative observation of converted phases, would support the concept of a mechanically detached lump of seismogenic material, but its origin and past history remain elusive.

Acknowledgements

Digital data used in the present study were obtained from the IRIS, GEOSCOPE and pIDC data centers. I am grateful to Paul Okubo at HVO and Olivier Hyvernaud at PPT for access to their respective analog archives. Numerous visits to the Caltech and Lamont–Doherty collections are also acknowledged. Dr. José Morales kindly provided the Andalusian records used in Section 4.7. Discussions with Steve Kirby, Craig Bina and Ray Russo are gratefully acknowledged. I thank Paul Lundgren and Rob van der Hilst for constructive comments on a previous version of the paper, and Renata Dmowska for a personalized international library loan. This study was supported in part by the National Science Foundation under grants EAR-93-16396 and EAR-97-06152, and by the Department of Defense, under grant DTRA-01-00-C0065. Many figures were drafted using the GMT software (Wessel and Smith, 1991).

Appendix A

We present here a detailed discussion of various events and records used in this study.

A.1. Kuril–Sakhalin subduction zone

A.1.1. Sea of Okhotsk, 30 August 1970; 52.4°N, 151.69°E; 645 km; $M_0 = 1.1 \times 10^{27}$ dyn cm

This deep event, studied by, among others, Strelitz (1980) and Sasatani (1980), and more recently, Huang and Okal (1998), is one of the largest recorded at depth under the Sea of Okhotsk. We document T waves at four short-period stations in the Pacific Basin: KIP, AFI and RAR (WWSSN), and PMO (Rangiroa). Note that "T wave channels" were not yet operational in Polynesia in 1970. Records at RAR and AFI are arguably faint, but their spectral characteristics establish them beyond any possible doubt as high-frequency waves without counterparts in the time series for that day, and thus as T phases. That they are at all legible

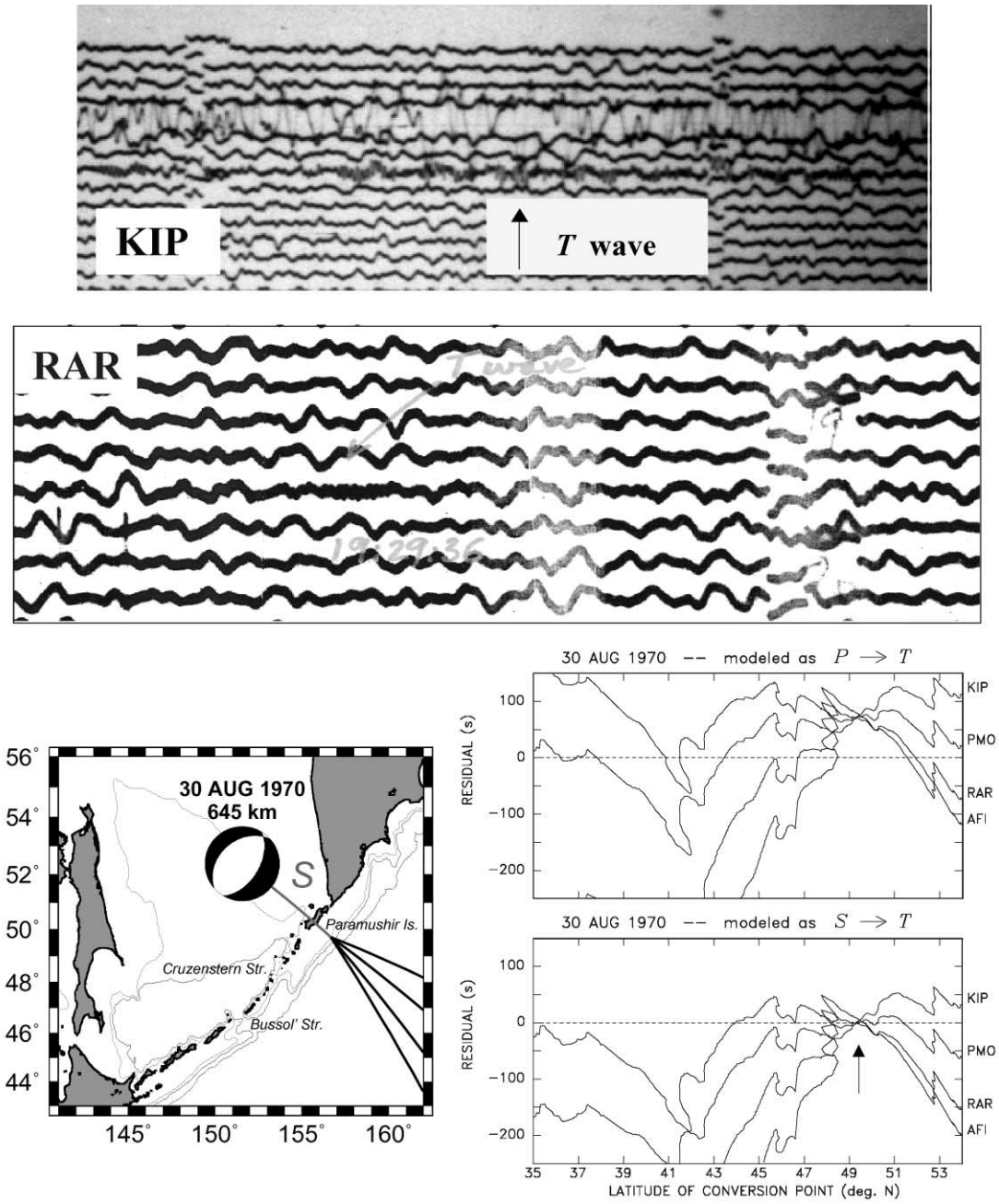

Fig. 16. Examples of T waves recorded on short-period channels of the WWSSN following the large 1970 Sea of Okhotsk deep shock. Top: record at Kipapa, Oahu. The duration of the window is 97 s and the original magnification of the record 12,500. The T wave is clearly apparent three traces below (i.e. 45 mn after) the prominent body waves. Bottom: record at Rarotonga. The duration is 56 s. Note the unmistakingly high-frequency character of the arrival, which emerges from the noise level despite a particularly mediocre gain at that station (originally 6250 at 1 Hz). The geometry of the conversion is shown on the bottom left map (similar to Fig. 3) and its nature as $S \rightarrow T$ established in the diagrams at bottom right (similar to Fig. 2).

on WWSSN records written at the mediocre magnifications used (6250 at RAR; Fig. 16) suggests a very strong acoustic wave. The record at KIP is clearer, with an estimated peak-to-peak amplitude of ground motion of 7 μm, a remarkable figure for a wave having travelled at least 40 km inside the structure of Oahu before reaching the station.

While in principle, it would be possible to interpret each arrival as resulting from a $P \rightarrow T$ conversion at an individual point of the Kuril coast (ranging from 47°N for PMO to 52°N for RAR), it is possible to model all four arrivals by diffraction of an S wave incident at 49.5°N, 156.3°E, off Paramushir Island (arrow in Fig. 16). This model is supported by a very favorable radiation of SV energy by the source towards the conversion point ($R^{SV} = 0.90$).

A.1.2. Sea of Okhotsk, 5 September 1970; 52.1°N, 150.99°E; 561 km; $M_0 = 6.4 \times 10^{25}$ dyn cm

For this aftershock of the previous event, we could find only one T phase, at PMO. The arrival time requires a much more southerly $S \rightarrow T$ conversion, at 46.5°N, 151.5°E, off the Bussol' Straits, which is easily explained by the difference in focal mechanism between the two shocks (Huang et al., 1997).

A.1.3. Sea of Okhotsk, 29 January 1971; 51.73°N, 150.95°E; 524 km; $M_0 = 2.5 \times 10^{26}$ dyn cm

We obtained two clear arrivals at KIP, separated by 108 s, and one at RAR. The record at PMO was noisy and could not be used. The T phase at KIP is interpreted as converted to P_n on the northern coast of Kauai, and corrected for the subsequent 199 km to the station. The travel-times are consistent with a common $S \rightarrow T$ scatterer to KIP and RAR at 46.8°N, 152.3°E, near the Bussol' Straits, and a conversion farther North, off Cruzenstern Straits (48.3°N, 153.9°E) for the $P \rightarrow T$ phase at KIP.

A.1.4. Sea of Okhotsk, 21 December 1975; 51.84°N, 151.75°E; 545 km; $M_0 = 2.1 \times 10^{26}$ dyn cm

We read two arrivals at PMO, and a clear one at KIP. They are interpreted as $P \rightarrow T$ and $S \rightarrow T$ conversions to PMO at Bussol' Straits (46.6°N, 151.5°E). The same $S \rightarrow T$ scatterer can be invoked on the path to KIP if an allowance is made for conversion back to P_n on the northern shore of Kauai.

A.1.5. Sea of Okhotsk, 21 June 1978; 47.98°N, 149.01°E; 402 km; $M_0 = 6.5 \times 10^{25}$ dyn cm

We obtained T phase doublets at both PMO and PPT, separated by 81 and 79 s, respectively. They are readily interpreted as conversions from a $P \rightarrow T$ scatterer at 45°N, 149.7°E (off Iturup), and an $S \rightarrow T$ one farther South off the Catherine Straits, at 44°N, 148°E.

A.1.6. Sea of Okhotsk, 10 July 1976; 47.36°N, 145.72°E; 421 km; $M_0 = 1.9 \times 10^{2}5$ dyn cm

The record at PMO shows two arrivals of fair quality, which can be interpreted as $P \rightarrow T$ and $S \rightarrow T$ conversions, respectively, off Shikotan Island (43.5°N, 147°E) and Nemuro Peninsula (42.9°N; 145.7°E).

A.1.7. Sea of Okhotsk, 1 February 1984; 49.10°N, 146.31°E; 581 km; $M_0 = 3.6 \times 10^{25}$ dyn cm

A double arrival at PMO is readily interpreted as $P \rightarrow T$ and $S \rightarrow T$ conversions South of Nemuro (42.6°N, 145°E). The record at TBI could not be easily interpreted.

A.1.8. Sea of Okhotsk, 18 May 1987; 49.12°N, 147.39°E; 552 km; $M_0 = 1.7 \times 10^{26}$ dyn cm

This earthquake generated exceptionally long T wavetrains at PMO. The first arrival is readily identified as a $P \rightarrow T$ conversion at Bussol' Straits, but the interpretation of the later arrivals requires multipathing through many conversion points along the southern Kuril arc. Because we cannot assertively demonstrate the occurrence of an $S \rightarrow T$ conversion, we show this event as an open star in Fig. 4.

A.1.9. Primorye, 21 July 1994; 42.3°N, 132.9°E; 471 km; $M_0 = 1.1 \times 10^{27}$ dyn cm

Finally, we complete here the investigation of this strong event under the Primorye province of eastern Russia, whose record at RPN was used in the introduction to illustrate our methodology. Most other stations in the Pacific Basin recorded T phases. We identified $S \rightarrow T$ conversions at KOS, NAU, RAR, TET, PMO and RPN, with NAU and RPN showing earlier $P \rightarrow T$ phases. The conversion points are located on a 150 km stretch of the northernmost shore of Honshu (Fig. 3).

A.2. Bonin–Marianas arc

We start with a discussion of events located at a similar latitude to the 1982 "detached" earthquake, but in the mainstream WBZ.

A.2.1. Bonin Islands, 3 May 1991; 28.14°N, 139.65°E; 453 km; $M_0 = 1.3 \times 10^{26}$ dyn cm

The T wave channel at PMO saturated, but the regular seismic channel recorded a superb wavepacket, composed of two arrivals, generally similar to those from the 1982 event shown in Fig. 6. They are easily interpreted as $P \rightarrow T$ and $S \rightarrow T$ conversions at either Iwo Jima or Muka Jima.

Despite significant background noise at Easter Island (RPN), spectrogram techniques extract a T arrival at 04:48:35 GMT, in the 3–4 Hz frequency band. This signal is interpreted as an $S \rightarrow T$ conversion at Haha Jima, reflected on the northwestern Hawaiian Islands. The exact location of the reflector cannot be further constrained.

A.2.2. Bonin Islands, 13 May 1977; 28.12°N, 139.73°E; 440 km; $M_0 = 6.1 \times 10^{25}$ dyn cm

Results are similar to those of the previous shock: a double arrival at PMO interpreted as $P \rightarrow T$ and $S \rightarrow T$ conversions at either Iwo Jima or Chichi Jima.

A.2.3. Bonin Islands, 31 January 1973; 28.18°N, 138.86°E; 506 km; $M_0 = 2.5 \times 10^{26}$ dyn cm

We could obtain only one record, at PMO, on the regular seismic channel. A prominent arrival at 22:36:45, corresponding to $P \rightarrow T$ conversion at Iwo Jima or Chichi Jima, is followed by sustained high-frequency energy, from which no distinctive second arrival can be extracted. This event is shown as a yellow star in Fig. 6.

- To the North of the Bonin Islands, we examine the following events:
  - *Izu trench, 6 March 1984; 29.60°N, 139.11°E; 446 km; $M_0 = 1.4 \times 10^{27}$ dyn cm*

    This earthquake (the largest deep CMT solution in the Bonin–Mariana arc) generated spectacular T phases in Polynesia, which saturated the T wave channel at PMO for 10 min. The regular channels allow the identification of the strongest arrival at 03:59:35, with a precursor triggering saturation of the T wave channel at 03:58:12. These two times are readily interpreted as $P \rightarrow T$ and $S \rightarrow T$ paths converted either on the northern Bonin or northern Volcano Islands. Similarly, a powerful arrival at RKT is well matched by a $P \rightarrow T$ conversion at Muko Jima, the northernmost Bonin Island.

    A very intense T phase is present at TBI, even though the station is masked by the western Marshall Islands. The arrival time of the maximum amplitude, 04:12:35 GMT, could correspond to a reflection on Johnston Atoll (16.7°N; 169.5°W) for an $S \rightarrow T$ conversion at Haha Jima.
  - *Bonin Islands, 16 March 1996; 28.98°N, 138.94°E; 477 km; $M_0 = 1.1 \times 10^{26}$ dyn cm*

    Despite the size of this event, we could not identify T wave signals above noise level at any of the following stations: KIP, RAR, SNCC, PPT. A strong signal at SCZ, at 23:44:57, could be interpreted as a T wave converted from S at Haha Jima at the southern end of the Bonin Islands (26.3°N; 142.4°E). This interpretation remains speculative in the absence of corroborative signals in California (e.g. SNCC). We obtained a distinct doublet at WK30, readily interpreted as $P \rightarrow T$ and $S \rightarrow T$ converted at Muko Jima; these arrivals cannot be explained by conversion at the Volcano group. This event is shown as the purple star in Fig. 6.
  - *Bonin Islands, 5 August 1990; 29.48°N, 137.50°E; 520 km; $M_0 = 5.7 \times 10^{25}$ dyn cm*

    We obtained a small but distinctive doublet on the T wave channel at PMO, interpreted as $P \rightarrow T$ and $S \rightarrow T$ conversions at either Iwo Jima or Muko Jima. No other signal could be convincingly read at other stations. We show this event as a yellow star in Fig. 6.
  - *Izu Islands, 11 October 1993; 32.12°N, 138.02°E; 364 km; $M_0 = 2.5 \times 10^{26}$ dyn cm*

    This large event, about half-way between the Bonin Islands and Japan, produced a singular pattern of T waves. The PMO record in Polynesia shows a series of arrivals, the first one being the familiar $S \rightarrow T$ conversion at Haha Jima, but the most intense one, at 17:40:29 GMT, being too late to fit conversion anywhere along the islands or shallow seamounts of the Izu–Bonin arc. Rather, it can be successfully modeled by

a $P \rightarrow T$ conversion off the southeastern extremity of Honshu. Similarly, the main doublet of arrivals at RAR is best explained by $P \rightarrow T$ conversions on the coasts of Iwase (southern Honshu) and farther West off Murotozaki (Shikoku). This event is shown as the green star in Fig. 6.

- To the South of the Bonin Islands, we investigate the following events:
  - *Mariana Islands, 18 May 1979; 23.94°N, 142.66°E; 581 km;* $M_0 = 5.5 \times 10^{25}$ *dyn cm*

    A very weak T wave is readable on the T wave channel at PMO, at 21:58:18, and is readily interpreted as a $P \rightarrow T$ conversion, at either Iwo Jima or Haha Jima. No distinctive second arrival can be identified in the subsequent part of the record. We show this event as a brown star in Fig. 6.
  - *Mariana Islands, 23 August 1995; 18.88°N, 145.30°E; 599 km;* $M_0 = 4.6 \times 10^{26}$ *dyn cm*

    We could not find any definitive T wave record from this large deep event, despite examining data from TBI, PPT, KIP, RAR. We show this event as a black star in Fig. 6.
  - *Mariana Islands, 4 January 1982; 17.92°N, 145.46°E; 595 km;* $M_0 = 6.7 \times 10^{25}$ *dyn cm*

    A strong T phase is observed at PMO on the T wave channel, followed by several subsequent arrivals. The first signal corresponds to a $P \rightarrow T$ conversion on the eastern shore of Guam (13.6°N; 145.1°E). The latter arrivals could not be modeled assertively.

A.3. South America

A.3.1. Argentina, 23 June 1991; 26.8°S, 63.3°W; 558 km; $M_0 = 8.6 \times 10^{26}$ *dyn cm*

This is the largest deep Argentinian event with an available CMT solution. T waves were recorded in Hawaii (HUL), Easter (RPN), and Guam (GUMO). Significant volcanic activity at the Hollister Ridge during the relevant time window (Talandier and Okal, 1996) prevents the use of Polynesian stations. The HUL signal does not lend itself well to a clear separation into $P \rightarrow T$ and $S \rightarrow T$ arrivals (Fig. 8b). Based on comparisons with the other sources in the same region, we interpret the maximum in amplitude as an $S \rightarrow T$ conversion near Taltal, Chile (25.0°S; 70.6°W). The GUMO arrival is composed of a strong wavepacket lasting approximately 150 s, with maximum amplitude at 00:26:03 GMT on 24 June, with a smaller precursor at 00:23:47. We add a 4 s station correction at the receiver. These times then fit a $P \rightarrow T$ conversion at 27.2°S, 71.0°W, and an $S \rightarrow T$ one near Taltal (25.5°S). Finally, the RPN record shows a somewhat tentative arrival at 22:08:29 GMT. After applying a 3 s correction, this time fits an $S \rightarrow T$ conversion at 25.9°S; 70.8°W. Thus, most of the T phases recorded from this event would evolve from scatterers located along the bight offshore from Taltal, and activated by the S wave, 191 s after the origin time of the earthquake.

A.3.2. Argentina, 21 December 1983; 28.2°S, 63.2°W; 602 km; $M_0 = 2.7 \times 10^{26}$ *dyn cm*

This large event occurred at 12:05:06 GMT and was followed by an aftershock (no CMT available) at 12:15:07 GMT. Both shocks were well recorded at HUL on the southern shore of the Big Island of Hawaii, despite interference with local seismicity. Arrival times for the first event are easily interpreted as $P \rightarrow T$ and $S \rightarrow T$ conversions at 25.3 and 25.0°S, respectively. For the aftershock, the arrival corresponds to the $S \rightarrow T$ conversion; the expected $P \rightarrow T$ conversion is obscured by a local earthquake (Fig. 8a).

A.3.3. Argentina, 29 April 1994; 28.51°S, 63.22°W; 566 km; $M_0 = 2.5 \times 10^{26}$ *dyn cm*

The $S \rightarrow T$ conversion is well recorded at HUL, while the $P \rightarrow T$ one is much fainter (Fig. 8c). Scatterers are modeled at 23.7°S (P) and 24.0°S (S). No definitive T phases from this event were identified elsewhere in the Pacific Basin.

A.3.4. Argentina, 10 May 1994; 28.50°S, 63.10°W; 600 km; $M_0 = 2.8 \times 10^{26}$ *dyn cm*

The HUL record, shown in Fig. 8d, shows a faint $P \rightarrow T$ conversion and a better developed $S \rightarrow T$ one. The scatterers are located to the North at 23.7°S (P) and 24.6°S (S). In addition, we obtained a clear doublet at KOS, with scatterers at 30.2°S (P) and 28.3°S (S).

A.3.5. Argentina, 19 August 1994; 26.72°S, 63.42°W; 563 km; $M_0 = 5.6 \times 10^{25}$ dyn cm

With this event, we reach what we regard as the limit of detectability at HUL (Fig. 8e). By analogy with the previous events, we believe that the faint signal at 12:02:03 GMT corresponds to an $S \rightarrow T$ conversion, which would then involve a scatterer at 23.8°S, 70.6°W. We could not extract definite signals at other Pacific sites.

A.3.6. Paraguay, 15 April 1969; 21.86°S, 61.68°W; 541 km; $m_b = 4.0$

We relocated this small earthquake just 10 km to the North; Monte Carlo relocations with a generous noise ($\sigma_G = 1.5$ s) are not sufficient to bring it into the mainstream WBZ, while keeping its depth robust (521–574 km). We conclude that the earthquake is indeed an outboard outlier. It remains much too small for a study of any possible *T* waves.

A.3.7. Argentina, 8 February 1965; 23.1°S, 62.5°W; 468 km; $m_b = 4.7$

The above NEIC location stands out, while the ISC location is in the mainstream WBZ. We also relocate the earthquake in the WBZ, and at a significantly greater depth (22.47°S; 63.49°W; 547 km), a hypocenter close but not identical to that of a foreshock 2 min earlier.

A.3.8. Argentina, 25 February 1964; 22.2°S, 62.6°W; 470 km; $m_b = 4.1$

The NEIC location is outboard, but the dataset has poor longitudinal resolution. The Monte Carlo ellipse drawn with very little noise ($\sigma_G = 1$ s) intersects the mainstream WBZ. Our preferred location (22.29°S; 62.94°W) also involves a greater depth (506 km).

A.3.9. Argentina, 10 June 1964; 22.5°S, 64.7°W; 480 km; no magnitude reported

The above NEIC location would make this an "inboard outlier" to the West of the WBZ. While our relocation converges on the same solution, the dataset has poor resolution in the ESE–WNW direction, and the 1 s ellipse intersects the mainstream WBZ.

A.3.10. Argentina, 9 February 1926; 27°S, 59.5°W; 540 km; $M_{PAS} = 6$

The above ISS location would qualify as an outboard hypocenter, although Gutenberg and Richter's (1954) solution (28°S; 62°W) lies within the WBZ. We relocate the event even farther West (28.57°S; 62.68°W), at the very bottom of the active WBZ (626 km).

A.3.11. Chile, 18 September 1975; 34.15°S, 68.90°W; 429 km; no magnitude reported

If its location were confirmed, this small earthquake would represent an event detached both vertically and horizontally, in a section of the Andean subduction zone where no deep seismicity is otherwise observed. We relocate the earthquake even farther South (35.46°S; 67.67°W; 465 km), but note that the dataset has only 5 *P* times, with the Monte Carlo ellipsoid ($\sigma_G = 1.5$ s) intersecting the active WBZ at intermediate depths.

References

Adams, R.D., 1963. Source characteristics of some deep New Zealand earthquakes. N.Z. J. Geol. Geophys. 6, 209–220.

Adams, R.D., Ferris, B.G., 1976. A further earthquake at exceptional depth between New Zealand. N.Z. J. Geol. Geophys. 9, 269–273.

Barazangi, M., Isacks, B., Oliver, J., 1972. Propagation of seismic waves through and beneath the lithosphere that descends under the Tonga Island arc. J. Geophys. Res. 77, 952–958.

Bellon, H., 1981. Chronologie radiométrique (K–Ar) des manifestations magmatiques autour de la Méditerraneé occidentale entre 33 et 1 Ma. In: Wezel, F.C. (Ed.), Sedimentary Basins of Mediterranean Margins, Tecnoprint, Bologna, pp. 341–360.

Benioff, H., 1949. Seismic evidence for the fault origin of oceanic deeps. Geol. Soc. Amer. Bull. 60, 1837–1856.

Bina, C.R., 1997. Patterns of deep seismicity reflect buoyancy stresses due to phase transitions. Geophys. Res. Lett. 24, 3301–3304.

Blanco, M.J., Spakman, W., 1993. The *P* wave velocity structure of the mantle below the Iberian Peninsula: evidence for subducted lithosphere below southern Spain. Tectonophysics 221, 13–34.

Brudzinski, M.R., Chen, W.-P., 1998. Anomalous seismicity disassociated with high *P* wave speeds in the transition zone beneath the Tonga back-arc, Eos. Trans. Am. Geophys. Union, 79 (45) F633 (abstract).

Buforn, E., Udías, A., Mezcua, J., Madariaga, R., 1991. A deep earthquake under south Spain, 8 March 1990. Bull. Seismol. Soc. Am. 81, 1403–1407.

Buforn, E., Coca, P., Udías, A., Lasa, C., 1997. Source mechanism of intermediate and deep earthquakes in southern Spain. J. Seismol. 1, 113–130.

Chung, W.-Y., Kanamori, H., 1976. Source process and tectonic implication of the Spanish deep-focus earthquake of March 29, 1954. Phys. Earth Planet. Int. 13, 85–96.

DeMets, D.C., Gordon, R.G., Argus, D.F., Stein, S., 1990. Current plate motions. Geophys. J. Intl. 101, 425–478.

Engdahl, E.R., van der Hilst, R., Berrocal, J., 1995. Imaging of subducted lithosphere beneath South America. Geophys. Res. Lett. 22, 2317–2320.

Engdahl, E.R., van der Hilst, R., Buland, R., 1998. Global teleseismic earthquake relocation with improved travel-times and procedures for depth determination. Bull. Seismol. Soc. Am. 88, 722–743.

Engebretson, D.C., Kirby, S.H., 1992. Deep Nazca slab seismicity: why is it so anomalous? Eos. Trans. Am. Geophys. Union 73 (43) 379 (abstract).

Ewing, W.M., Woollard, G.P., Vine, A.C., Worzel, J.L., 1946. Recent results in submarine geophysics. Geol. Soc. Am. Bull. 57, 909–934.

Fukao, Y., Obayashi, M., Inoue, H., Nenbai, M., 1992. Subducting slabs stagnant in the mantle transition zone. J. Geophys. Res. 97, 4809–4822 .

Glennon, M.A., Chen, W.-P., 1993. Systematics of deep-focus earthquakes along the Kuril–Kamchatka arc and their implications on mantle dynamics. J. Geophys. Res. 98, 735–769.

Grand, S.P., 1994. Mantle shear structure beneath the Americas and surrounding oceans. J. Geophys. Res. 99, 11591–11621.

Grimison, N.L., Chen, W.-P., 1986. The Azores–Gibraltar plate boundary: focal mechanisms, depths of earthquakes, and their tectonic implications. J. Geophys. Res. 91, 2029–2047.

Gutenberg, B., Richter, C.F., 1954. Seismicity of the Earth and Associated Phenomena. Princeton University Press, Princeton, NJ, 310 p.

Huang, W.-C., Okal, E.A., 1998. Centroid moment tensor solutions for deep earthquakes predating the digital era: discussion and inferences. Phys. Earth Planet. Inter. 106, 191–218.

Huang, W.-C., Okal, E.A., Ekström, G., Salganik, M.P., 1997. Centroid moment tensor solutions for deep earthquakes predating the digital era: the WWSSN dataset (1962–1976). Phys. Earth Planet. Int. 99, 121–129.

Huang, W.-C., Okal, E.A., Ekström, G., Salganik, M.P., 1998. Centroid moment tensor solutions for deep earthquakes predating the digital era: the historical dataset (1907–1961). Phys. Earth Planet. Int. 6, 181–190.

Isacks, B.L., Barazangi, M., 1973. High-frequency shear waves guided by a continuous lithosphere descending beneath western South America. Geophys. J. Roy. Astron. Soc. 33, 129–139.

Isacks, B.L., Molnar, P., 1971. Distribution of stresses in the descending lithosphere from a global survey of focal mechanism solutions of mantle earthquakes. Rev. Geophys. Space Phys. 9, 103–174.

Kagan, Y.Y., 1991. 3-D rotation of double-couple earthquake sources. Geoph. J. Intl. 106, 709–716.

Kirby, S.H., Durham, W.B., Stern, L.A., 1991. Mantle phase changes and deep-earthquake faulting in subducting lithosphere. Science 252, 216–225.

Kirby, S.H., Okal, E.A., Engdahl, E.R., 1995. The 9 June 1994 great Bolivian deep earthquake: an exceptional deep earthquake in an extraordinary subduction zone. Geophys. Res. Lett. 22, 2233–2236.

Kirby, S.H., Stein, S., Okal, E.A., Rubie, D., 1996. Deep earthquakes and metastable mantle phase transformations in subducting oceanic lithosphere. Rev. Geophys. Space Phys. 34, 261–306.

Kostoglodov, V.V., 1989. Maximal'naya glubina zemletryasenii i fazovye prevrashcheniya v litosfere, pograzhayushchejsya v mantiyu. In: Magnitskii, V.A. (Ed.), Fizika i vnutrennee stroienie zemli. Nauka, Moskva, pp. 52–57 (in Russian).

Levitus, S., Boyer, T.P., Antonov, J., Burgent, R., Conkright, M.E., 1994. World Ocean Atlas 1994, NOAA/NESDIS, Silver Spring, MD.

Lonergan, L., White, N., 1997. Origin of the Betic–Rif mountain belt. Tectonics 16, 504–522.

Lundgren, P.R., Giardini, D., 1994. Isolated deep earthquakes and the fate of subduction in the mantle. J. Geophys. Res. 99, 15833–15842.

Mele, G., 1998. High-frequency wave propagation from mantle earthquakes in the Tyrrhenian Sea: constraints for the geometry of the South Tyrrhenian subduction zone. Geophys. Res. Lett. 25, 2877–2880.

Mezcua, J., Rueda, J., 1997. Seismological evidence for a delamination process in the lithosphere under the Alborán Sea. Geophys. J. Intl. 129, F1–F8.

Mitchell, B.J., 1995. Anelastic structure and evolution of the continental crust and upper mantle from seismic surface wave attenuation. Rev. Geophys. 33, 441–462.

Mooney, H.M., 1970. Upper mantle inhomogeneity beneath New Zealand: seismic evidence. J. Geophys. Res. 75, 285–309.

Morales, J., Serrano, I., Jabaloy, A., Galindo-Zaldivar, J., Zhao, D., Torcal, F., Vidal, F., González-Lodeiro, F., 1999. Active continental subduction beneath the Betic Cordillera and the Alborán Sea. Geology 27, 735–738.

Okal, E.A., 1992. A student's guide to teleseismic body-wave amplitudes. Seismol. Res. Lett. 63, 169–180.

Okal, E.A., Bina, C.R., 1994. The deep earthquakes of 1921–1922 in northern Peru. Phys. Earth Planet. Int. 87, 33–54.

Okal, E.A., Bina, C.R., 2001. The deep earthquakes of 1997 in Western Brazil. Bull. Seismol. Soc. Amer., 91, 161–164.

Okal, E.A., Jo, B.-G., 1990. Q measurements for phase X overtones. Pure Appl. Geophys. 132, 331–362.

Okal, E.A., Kirby, S.H., 1998. Deep earthquakes beneath the North and South Fiji Basins, SW Pacific: Earth's most intense deep seismicity in stagnant slabs. Phys. Earth Planet. Int. 109, 25–63.

Okal, E.A., Talandier, J., 1997. T waves from the great 1994 Bolivian deep earthquake in relation to channeling of S wave energy up the slab. J. Geophys. Res. 102, 27421–27437.

Okal, E.A., Talandier, J., 1998. Correction to "T waves from the great 1994 Bolivian deep earthquake in relation to channeling of S wave energy up the slab". J. Geophys. Res. 103, 2793–2794.

Okal, E.A., Engdahl, E.R., Kirby, S.H., Huang, W.-C., 1995. Earthquake relocations in the Kuril slab: was the 1990 Sakhalin event not isolated after all? Eos. Trans. Am. Geophys. Union 76 (17), S199, (abstract).

Okino, K., Ando, M., Kaneshima, S., Hirahara, K., 1989. The horizontally lying slab. Geophys. Res. Lett. 16, 1059–1062.

Richardson, W.P., 1998. Surface-wave tomography of the Ontong–Java plateau: seismic probing of the world's largest igneous province. Ph.D. Thesis. Northwestern University, Evanston, IL, 191 p.

Royden, L.H., 1993. Evolution of retreating subduction boundaries formed during continental collision. Tectonics 12, 628–638.

Sacks, I.S., 1969. Distribution of Absorption of Shear Waves in South America, and Its Tectonic Significance. Vol. 67, Yearbook Carnegie Institute Washington, pp. 339–344.

Sasatani, T., 1980. Source parameters and rupture mechanism of deep-focus earthquakes. J. Fac. Sci. Hokkaido Univ. Ser. 7 Geophys. 6, 301–384.

Seber, D., Barazangi, M., Ibenbrahim, A., Demnati, A., 1996. Geophysical evidence for lithospheric delamination beneath the Alborán Sea and Rif–Betic mountains. Nature 379, 785–790.

Snoke, J.A., Sacks, I.S., Okada, H., 1974a. Empirical models for anomalous high-frequency arrivals from deep-focus earthquakes in South America. Geophys. J. Roy. Astron. Soc. 37, 133–139.

Snoke, J.A., Sacks, I.S., Okada, H., 1974b. A model not requiring continuous lithosphere for anomalous high-frequency arrivals from deep-focus South American earthquakes. Phys. Earth Planet. Int. 9, 199–206.

Strelitz, R.A., 1980. The fate of downgoing slab: a study of the moment tensors from body waves of complex deep-focus earthquakes. Phys. Earth Planet. Int. 21, 83–96.

Talandier, J., Kuster, G.T., 1976. Seismicity and submarine volcanic activity in French Polynesia. J. Geophys. Res. 81, 936–948.

Talandier, J., Okal, E.A., 1996. "Monochromatic *T* waves from underwater volcanoes in the Pacific Ocean: ringing witnesses to geyser processes". Bull. Seismol. Soc. Am. 86, 1529–1544.

Talandier, J., Okal, E.A., 1998. On the mechanism of conversion of seismic waves to and from *T* waves in the vicinity of island shores. Bull. Seismol. Soc. Am. 88, 621–632.

Taylor, R.N., Nesbitt, R.W., Vidal, P., Harmon, R.S., Auvray, B., Croudace, I.W., 1994. Mineralogy, chemistry and genesis of the Boninite series volcanics, Chichijima, Bonin Islands, Japan. J. Petrol. 35, 577–617.

Tracey Jr., J.I., Schlanger, S.O., Stark, J.T., Doan, D.B., May, H.G., 1964. General geology of Guam. US Geol. Surv. Prof. Paper 403-A, A1–A104.

Udías, A., López-Arroyo, A., Mezcua, J., 1976. Seismotectonics of the Azores–Alborán region. Tectonophysics 31, 259–289.

Umino, S., 1985. Volcanic geology of Chichijima, the Bonin Islands (Ogasawara Islands). J. Geol. Soc. Jpn. 91, 505–523.

Utsu, T., 1971. Seismological evidence for anomalous structures of island arcs with special reference to the Japanese region. Rev. Geophys. Space Phys. 9, 839–890.

Uyeda, S., Kanamori, H., 1979. Back-arc opening and the mode of subduction. J. Geophys. Res. 84, 1049–1061.

Van Ark, E., Marton, F., Stein, S., Bina, C., Rubie, D.C., 1999. Persistence of metastable olivine in detached slabs as a possible cause of deep earthquakes. In: Proceedings of the 1999 Alfred-Wegener Conference. Vol. 7, Terra Nostra, 1999, p. 106 (abstract).

van der Hilst, R., 1995. Complex morphology of subducted lithosphere in the mantle beneath the Tonga trench. Nature 374, 154–157.

van der Hilst, R.D., Snieder, R., 1996. High-frequency precursors to *P* wave arrivals in New Zealand: implications for slab structure. J. Geophys. Res. 101, 8473–8488.

van der Hilst, R.D., Engdahl, E.R., Spakman, W., Nolet, G., 1991. Tomographic imaging of subducted lithosphere below northwest Pacific island arcs. Nature 353, 37–43.

van der Hilst, R., Engdahl, E.R., Spakman, W., 1993. Tomographic inversion of *P* and *pP* data for aspherical mantle structure below the northwest Pacific region. Geophys. J. Intl. 115, 264–302.

Wessel, P., Smith, W.H.F., 1991. Free software helps map and display data. Eos. Trans. Am. Union 72, 441; 445–446.

Widiyantoro, S., Kennett, B.L.N., van der Hilst, R.D., 1997. Mantle structure beneath Indonesia inferred from high-resolution tomographic imaging. Geophys J. Intl. 130, 167–182.

Widiyantoro, S., Kennett, B.L.N., van der Hilst, R.D., 1999. Seismic tomography with *P* and *S* data reveals lateral variations in the rigidity of deep slabs. Earth Planet. Sci. Lett. 173, 91–100.

Wortel, M.J.R., 1984. Spatial and temporal variations in the Andean subduction zone. J. Geol. Soc. London 141, 783–791.

Wysession, M.E., Okal, E.A., Miller, K.L., 1991. Intraplate seismicity of the Pacific Basin, 1913–1988. Pure Appl. Geophys. 135, 261–359.